PAPER

Trees and spatial topology change in causal dynamical triangulations

J. Phys. A: Math. Theor. **46** (2013) 315201 (33pp) doi:10.1088/1751-8113/46/31/315201

Trees and spatial topology change in causal dynamical triangulations

J Ambjørn[1,2] **and T G Budd**[1]

[1] The Niels Bohr Institute, Copenhagen University, Blegdamsvej 17, DK-2100 Copenhagen Ø, Denmark
[2] Institute for Mathematics, Astrophysics and Particle Physics (IMAPP), Radbaud University Nijmegen, Heyendaalseweg 135, 6525 AJ, Nijmegen, The Netherlands

E-mail: ambjorn@nbi.dk and budd@nbi.dk

Received 11 February 2013, in final form 4 July 2013
Published 19 July 2013
Online at stacks.iop.org/JPhysA/46/315201

Abstract
Generalized causal dynamical triangulations (generalized CDT) is a model of two-dimensional quantum gravity in which a limited number of spatial topology changes is allowed to occur. We solve the model at the discretized level using bijections between quadrangulations and trees. In the continuum limit (scaling limit) the amplitudes are shown to agree with known formulas and explicit expressions are obtained for loop propagators and two-point functions. It is shown that from a combinatorial point of view generalized CDT can be viewed as the scaling limit of planar maps with a finite number of faces and we determine the distance function on this ensemble of planar maps. Finally, the relation with planar maps is used to illuminate the mysterious identity of certain continuum cylinder amplitudes.

PACS numbers: 04.60.Kz, 04.06.Nc, 02.10.Ox

(Some figures may appear in colour only in the online journal)

1. Introduction

Two-dimensional quantum gravity has been an important topic in theoretical physics for a long time. String theory *is* two-dimensional quantum gravity coupled to certain conformal field theories in its simplest perturbative formulation. When the central charge c of a conformal field theory is less than 1 the models correspond to non-critical string theories, and it is possible to solve certain aspects of the gravity-matter system analytically. Also, for $c < 1$ it is possible to provide a path integral regularization of these quantum theories. In this regularization one performs the integration over 2D geometries by summing over equilateral triangulations (so-called *dynamical triangulations* (DT)), eventually recovering the continuum limit by taking the length ϵ of the links to zero. Remarkably, a class of these regularized theories can be solved analytically, even for $\epsilon > 0$, using combinatorial techniques, either by directly counting certain

graphs or by using so-called matrix models. The outcome of this has been a beautiful Wilsonian picture where one has universality: the continuum limit is to a large extent independent of the details of the regularization. It does not really matter if the starting point is triangulations or one uses quadrangulations or higher order polygons in an arbitrary combination, as long as the weights of these are positive (see e.g. [2], chapter 4, for a review). Thus one has an infinite dimensional coupling constant space, the coupling constants being the relative weights of various types of polygons, and the critical surface where the continuum limit can be taken is a hyper-surface of finite co-dimension. On this hyper-surface one obtains 'pure' 2D Euclidean quantum gravity. If one allows negative weights for some polygons one can flow to new continuum theories describing 2D Euclidean quantum gravity coupled to various conformal matter theories, and if one allows for various 'flavors' to be attached to the polygons and a local interaction between these, one can obtain all minimal, rational conformal field theories coupled to 2D Euclidean quantum gravity in the continuum limit.

These 2D discretized models can be generalized to higher dimensions [1, 5]. However it has so far not been possible to find a *continuum limit* which can be viewed as higher dimensional quantum gravity. This failure triggered an attempt to define a new class of regularized models where the sums over the piecewise linear geometries were first carried out in spacetimes with Lorentzian signature and local causality was imposed. This class of piecewise linear geometries was denoted *causal dynamical triangulations* (CDT) [6, 8]. When rotating back to Euclidean signature, one is effectively summing over triangulations where there is a *proper time foliation*. It seems that this class of models has an interesting continuum limit both in three and four dimensions (for a review see [4]), but until now this has only been investigated using computer simulations (in three dimensions somewhat related models have been looked at analytically). Here we will concentrate on 2D where the regularized model can be solved analytically using combinatorial methods. More specifically we will consider a model known as *generalized CDT*, which interpolates between the CDT and DT models [10, 11]. In the generalized CDT model one starts out with space being connected, i.e. having the topology of S^1, and as a function of proper time one allows it to split into a finite number of S^1 components. Using recent combinatorial results we will solve the discretized model and show how one can obtain the scaling or continuum limit of the model. Further we will discuss how this limit relates to the standard CDT and DT limits. To simplify the discussion we use a model which at the discretized level is described by quadrangulations, rather than triangulations. (in section 7 we show how the results can be generalized to triangulations).

The rest of the paper is organized as follows: in section 2 we review how quadrangulations of the sphere are related to labeled planar trees in the case of DT and to unlabeled planar trees in the case of CDT. In section 3 we show how one can use these trees to study a discrete version of generalized CDT and how to find its scaling limit. A more detailed counting of labeled trees in section 4 allows us to study proper time dependences in generalized CDT. In section 5 it is shown that generalized CDT can also be interpreted as a scaling limit of random planar maps for which the number of faces is conditioned to remain finite.

There exists an intriguing identity between certain cylinder amplitudes in the scaling limit, first discussed in the context of DT by Kawai and Ishibashi [28] and later in the context of generalized CDT in [10]. Kawai and Ishabashi related the identities to a Virasoro algebra and an underlying conformal invariance, but in the context of generalized CDT the identities appeared quite mysterious. However, we will show that they are even valid at the discretized level and can be understood as a bijection between sets of quadrangulations defining the cylinder amplitudes in question. This is discussed in section 6.

Finally, in section 7 it is shown how some of the quadrangulation results can be generalized to triangulations.

2. Bijections

2.1. Definitions

In the following we will make extensive use of planar trees, quadrangulations, triangulations and more general tilings of the 2-sphere. In order to facilitate the discussion it is useful to recognize these objects as subclasses of the more general notion of planar maps.

An *embedded planar graph* is a multigraph, i.e. a graph in which edges are allowed to begin and end at the same vertex and in which multiple edges are allowed between pairs of vertices, embedded in the 2-sphere without crossing edges. A *planar map* is a connected embedded planar graph. Two planar maps are considered equivalent if they can be continuously deformed into each other. An equivalence class of planar maps can be described purely combinatorically, e.g. by labeling the vertices and writing down for each vertex an (clockwise) ordered list of its neighbors in the graph. The connected components of the complement of an embedded planar graph in the sphere are called the *faces* of the graph. In the case of a planar map all faces are topological disks and the number of edges bounding a face is called the *degree* of the face. A face of degree d also has d corners, where by a *corner* we mean a small sector around a vertex bounded by two consecutive edges of the face. Notice that a single vertex may appear more than once as a corner of a face.

When it comes to counting it is often convenient to deal with objects with no internal symmetries. In the case of planar maps, which may have a non-trivial automorphism group, the symmetry can be explicitly broken by *rooting* the map, which means that one marks an oriented edge, the *root edge*. The face directly to the left of the root edge is called the *root face* and its corner associated with the end of the root edge is the *root corner*. Clearly selecting a root edge is equivalent to selecting a root corner, and therefore either type of root may be used interchangeably.

Various classes of planar maps will be of interest to us. First of all, *triangulations* and *quadrangulations*, respectively, are planar maps for which each face has degree 3 and 4. More generally, a *p-angulation*, $p \geqslant 2$ is a planar map for which each face has degree p. A *p-angulation withb* boundaries of length l_i, $i = 1, \ldots, b$, is a planar map with b distinguished faces with degree l_i and all other faces having degree p. Finally, a *planar tree* is a planar map with only one face. The anti-clockwise ordered list of corners of the single face of a planar tree, starting at the root corner in the case of a *rooted planar tree*, is often called the *contour* of the tree. It corresponds to the (periodic) list of vertices one encounters when walking around the tree in a *clockwise* direction.

In the following we will often study *pointed quadrangulations*, which are quadrangulations with a marked vertex, called the *origin*. It is convenient to adopt a slightly different way of rooting a pointed quadrangulation, namely a *rooted pointed quadrangulation* is a pointed quadrangulation with a marked (unoriented) edge. As will become clear later, the marked vertex already induces a natural orientation on the edges and therefore a choice of orientation of the root edge would lead to a two-fold redundancy.

2.2. Cori–Vauquelin–Schaeffer bijection

The Cori–Vauquelin–Schaeffer bijection relates quadrangulations of the sphere with a marked vertex to planar trees with a labeling. Let us briefly describe the map and its inverse. For details and proofs we refer the reader to [22, 34, 37], or to section 5 where we discuss and prove a more general bijection.

Given a pointed quadrangulation of the sphere with N faces, we can label the vertices by their distance to the origin along the edges of the quadrangulation. The set of vertices

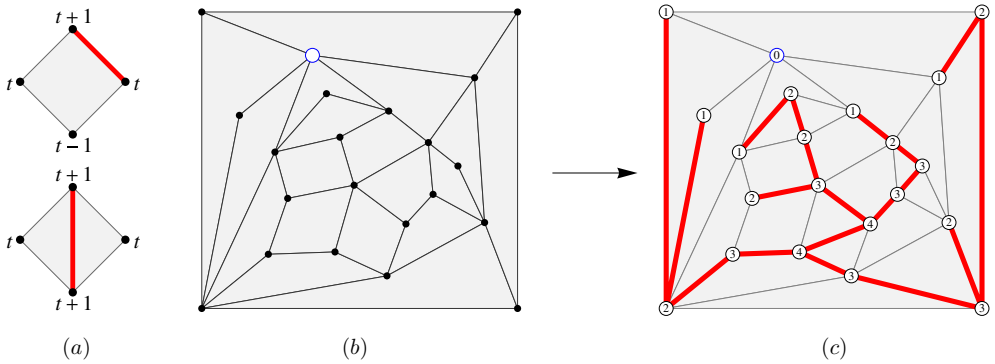

Figure 1. To every face of the quadrangulation one associates a colored edge depending on the labeling. The colored edges combine into a tree connecting all vertices except the origin.

naturally partitions into those with even, respectively odd, labels. As a consequence of the faces having an even number of sides, this partition turns the edge graph into a bipartite graph, i.e. vertices with even label only connect to vertices with odd label and vice versa. Hence, each edge connects vertices with labels differing by exactly 1. Taking into account the labeling, two types of faces occur in the quadrangulation, *simple* faces with labels $(t-1, t, t+1, t)$ and *confluent* faces with labels $(t+1, t, t+1, t)$ in cyclic order (see figure 1(a) and [22, 37]). A graph is drawn on the sphere by coloring the diagonal of each confluent face and the side of each simple face according to the prescription shown in figure 1(a). The resulting graph is a tree (with N edges) containing all the vertices of the quadrangulation except for the origin. This is a consequence of the following lemma, which we formulate more generally than necessary here, since we will be reusing this result in section 5.

Lemma 1. *Let Q be a quadrangulation with N faces and integer labels on its vertices, such that the labels differ by exactly 1 along the edges. Then the embedded planar graph $\mathcal{G}$ resulting from the prescription in figure 1(a) is connected and therefore a planar map. Moreover, each face of $\mathcal{G}$ contains in its interior exactly one vertex of Q. These vertices are exactly the local minima of the labeling, i.e. vertices whose labels are smaller or equal to all the labels of their neighbors.*

Proof. First we show that a vertex of Q is a vertex of $\mathcal{G}$ if and only if it is not a local minimum. Since the coloring in figure 1(a) stays away from the minimal labels in the quadrangles, it is clear that a local minimum is not a vertex of $\mathcal{G}$. Given a vertex v of Q labeled t that is not a local minimum, one can find an edge running from v to a vertex labeled $t-1$. By inspection of figure 1(a) we see that the quadrangle directly to the right of this edge in any case gives rise to a colored edge ending at v.

Let us now prove that each face $\mathcal{F}$ of the embedded planar graph contains a vertex that is a local minimum. For a given face $\mathcal{F}$, select from its corners one which has smallest possible label t. There must exist an edge leading away from this vertex and having $\mathcal{F}$ on its left-hand side. This edge ends at a vertex that is labeled either t or $t+1$. In the former case the edge is the diagonal of a confluent quadrangle, while in the latter case it is adjacent to a simple quadrangle on the left. As can be seen from figure 1(a), in either case the quadrangle contains a vertex with label $t-1$ lying to the left of the edge. Since this vertex cannot be a corner of $\mathcal{F}$

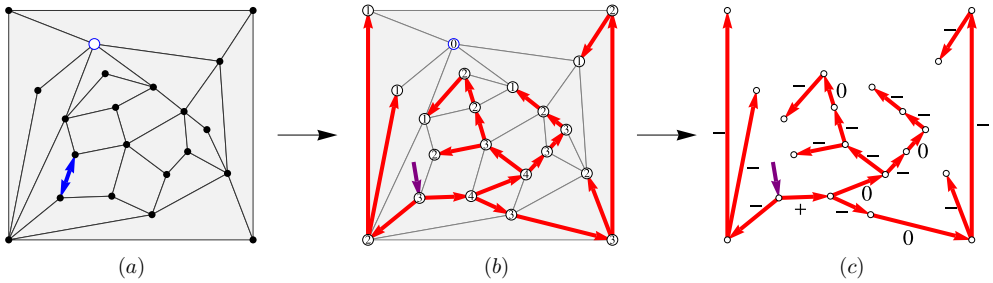

Figure 2. Rooted quadrangulations with an origin are in bijection with rooted planar trees labeled by $+, 0, -$.

it must lie in the interior of $\mathcal{F}$. Hence, there must be at least one local minimum in the interior of $\mathcal{F}$.

Let V, E and F be the number of vertices, edges and faces of $\mathcal{G}$, respectively. The number of vertices of Q is $N + 2$, which follows from the Euler formula, and each vertex of Q that is not a local minimum belongs to $\mathcal{G}$, therefore $V = N - N_{\min} + 2$. By construction $E = N$ and from the considerations above it follows that $F \leqslant N_{\min}$. Therefore we have $V - E + F = F - N_{\min} + 2 \leqslant 2$. However, according to the Euler characteristic for embedded planar graphs[3] we have $V - E + F = 1 + C$, where $C \geqslant 1$ is the number of connected components of $\mathcal{G}$. The only solution is $C = 1$ and $F = N_{\min}$. We conclude that $\mathcal{G}$ is connected and that each face of $\mathcal{G}$ contains exactly one local minimum in its interior. □

Since the distance labeling has only one local minimum, namely the origin itself, application of the lemma shows that the colored graph is a planar map with a single face, hence a planar tree. Keeping the labels on the vertices one ends up with a *well-labeled tree*, i.e. a planar tree with positive integers on its vertices, such that at least one vertex is labeled 1 and the labels differ by at most one along its edges.

The quadrangulation can be reconstructed from the well-labeled tree in the following way. First we add by hand a new vertex in the plane, which will be the origin. Then we consider the *contour*, as defined above, containing the $2N$ corners of the tree in clockwise order. For every corner in the contour we draw a new edge in the plane: if the corner is labeled 1 we connect it to the origin; otherwise we connect it to the first corner following it that has smaller label. Up to deformations there is a unique way of drawing all these edges without crossings. After deleting the tree we are left with the original quadrangulation embedded in the plane. For a proof of these statements see theorem 1 in section 5.

The bijection can be extended to the rooted versions of the quadrangulations and trees described above. Recall that a rooted pointed quadrangulation is a pointed quadrangulation where one of the edges is marked (indicated by a double-sided arrow in figure 2(a)). Since the edges of the quadrangulation are in one-to-one correspondence with the corners in the contour of the tree, we obtain a distinguished corner which we take to be the *root* of the tree (indicated by a dark arrow in figure 2(b)). In a rooted tree all edges have a natural orientation, i.e. pointing away from the root. To each edge of the tree we associate a label $+$, 0 or $-$, depending on whether the label increases, remains the same, or decreases along the edge (see figure 2(c)).

[3] Recall from section 2.1 that the number of faces F of an embedded planar graph is the number of connected components of the complement of the graph in the sphere. With this definition Euler's formula $V - E + F = 2$ for connected embedded graphs generalizes to $V - E + F = 1 + C$ for embedded planar graphs with C connected components.

These labels are sufficient to reconstruct the labels on the vertices, since by construction the minimal label on the vertices is fixed to be equal to 1. From these constructions it follows that rooted pointed quadrangulations with N faces are in bijection with rooted planar trees with N edges labeled by $+$, 0, $-$ (see [22], theorem 4).

Notice that this bijection makes the counting of quadrangulations extremely simple. Rooted planar trees with N edges are counted by the Catalan numbers

$$C(N) = \frac{1}{N+1}\binom{2N}{N}, \tag{1}$$

while the number of labelings is simply 3^N. The generating function $z^{(\ell)}(g)$ for the number of well-labeled rooted planar trees, and also for the number of rooted pointed quadrangulations, is therefore given by

$$z^{(\ell)}(g) = \sum_{N=0}^{\infty} 3^N C(N) g^N = \frac{1-\sqrt{1-12g}}{6g}. \tag{2}$$

Since a quadrangulation of the sphere with N faces has $2N$ edges and $N+2$ vertices, the micro-canonical partition function for unmarked quadrangulations is

$$Z(N) = \sum_{Q} \frac{1}{C_Q} = \frac{3^N}{2N(N+2)} C(N) = \frac{1}{2\sqrt{\pi}} N^{-7/2} 12^N (1 + \mathcal{O}(N^{-1})), \tag{3}$$

where C_Q is the order of the automorphism group of the quadrangulation Q.

2.3. Causal triangulations

A similar bijection between causal triangulations and trees has been used in [26, 31, 35] and earlier in a slightly different form in [25]. In analogy with the quadrangulations in the previous section we can define causal triangulations, which were introduced in [8], in the following way. Consider a triangulation of the sphere with a marked vertex (the black point in figure 3(*a*)), which we call the origin. We interpret the labeling of the vertices that arises from the distance to the origin as a time function, the CDT time. The edges of the triangulation come in two types: *spacelike* edges connecting vertices with identical labels and *timelike* edges connecting vertices with different labels (dashed, resp. solid, edges in figure 3(*a*)). A triangulation with origin is a *causal triangulation* when the graph consisting of only the spacelike edges is a disjoint union of cycles and there is exactly one vertex with maximal label. In other words, the spatial topology as function of CDT time is fixed to be S^1.

Since every triangle in a causal triangulation is bordered by exactly one spacelike edge, there is a canonical pairing of triangles sharing a spacelike edge. By joining all these pairs of triangles into faces, in other words, by deleting the spacelike edges, we end up with a quadrangulation of the sphere (figure 3(*b*)). Notice that the removal of the spacelike edges has no effect on the distance labeling, because by construction they connect vertices with identical labels. Therefore the CDT time on the quadrangulation corresponds exactly to the labeling in the context of the Cori–Vauquelin–Schaeffer bijection. The class of quadrangulations, which we call *causal quadrangulations*, arising from this construction is easily seen to be characterized by the presence of a unique local maximum of the labeling.

If we root the pointed quadrangulation at one of the edges incident to the maximal vertex and apply Schaeffer's prescription, we end up with a rooted planar tree with all edges labeled by $-$ (figure 3(*c*)). A direct consequence is that rooted causal quadrangulations with N faces, and also rooted causal triangulations with $2N$ triangles, are counted by the Catalan numbers

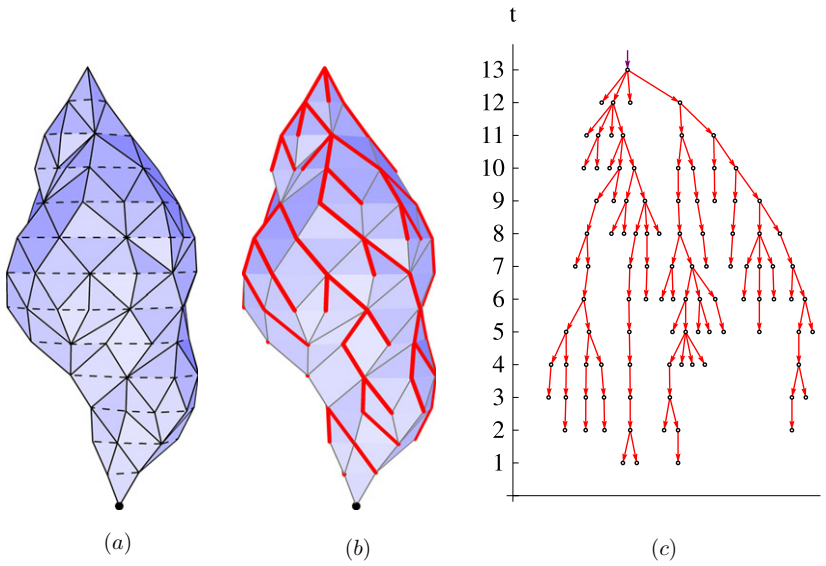

Figure 3. From (*a*) causal triangulations to (*b*) causal quadrangulations to (*c*) unlabeled planar trees.

$C(N)$. Their generating function is identical to the generating function $z^{(u)}(g)$ of unlabeled trees,

$$z^{(u)}(g) = \sum_{N=0}^{\infty} C(N) g^N = \frac{1-\sqrt{1-4g}}{2g}. \tag{4}$$

Later we will see how adding a coupling associated with the labeling allows us to get causal quadrangulations and unrestricted quadrangulations as special cases of a more general model of random trees. But first let us show how one can extract more non-trivial scaling information from these representations by allowing quadrangulations with boundaries.

2.4. Quadrangulations with a boundary

As is shown in [16, 20, 23] the Cori–Vauquelin–Schaeffer bijection extends in a natural way to quadrangulations with a boundary. According to our definition in section 2.1 these are represented by planar maps of which all but one of the faces have degree 4. Quadrangulations with one boundary necessarily have even boundary length, which we denote by $2l$. An example of a quadrangulation with a boundary of length 28 is shown in figure 4(*a*). It is convenient to root the quadrangulation by selecting a corner of the boundary face (indicated by an arrow in figure 4(*a*)). As before, one of the vertices is marked as the origin, which may lie on the boundary.

Applying Schaeffer's prescription to the distance labeling we obtain a *forest* $\mathcal{F}$, i.e. a set of disjoint trees (figure 4(*b*)), instead of a single tree in the no-boundary case. Let us orient the boundary of the quadrangulation in a clockwise direction. Then to each boundary edge we can assign a $+$ or $-$ according to whether the label increases or decreases along the edge. It turns out that each tree contains exactly one vertex that is the end point of a $+$-edge. This was shown in [20], section 3.1, using a general bijection between planar maps and so-called *labeled*

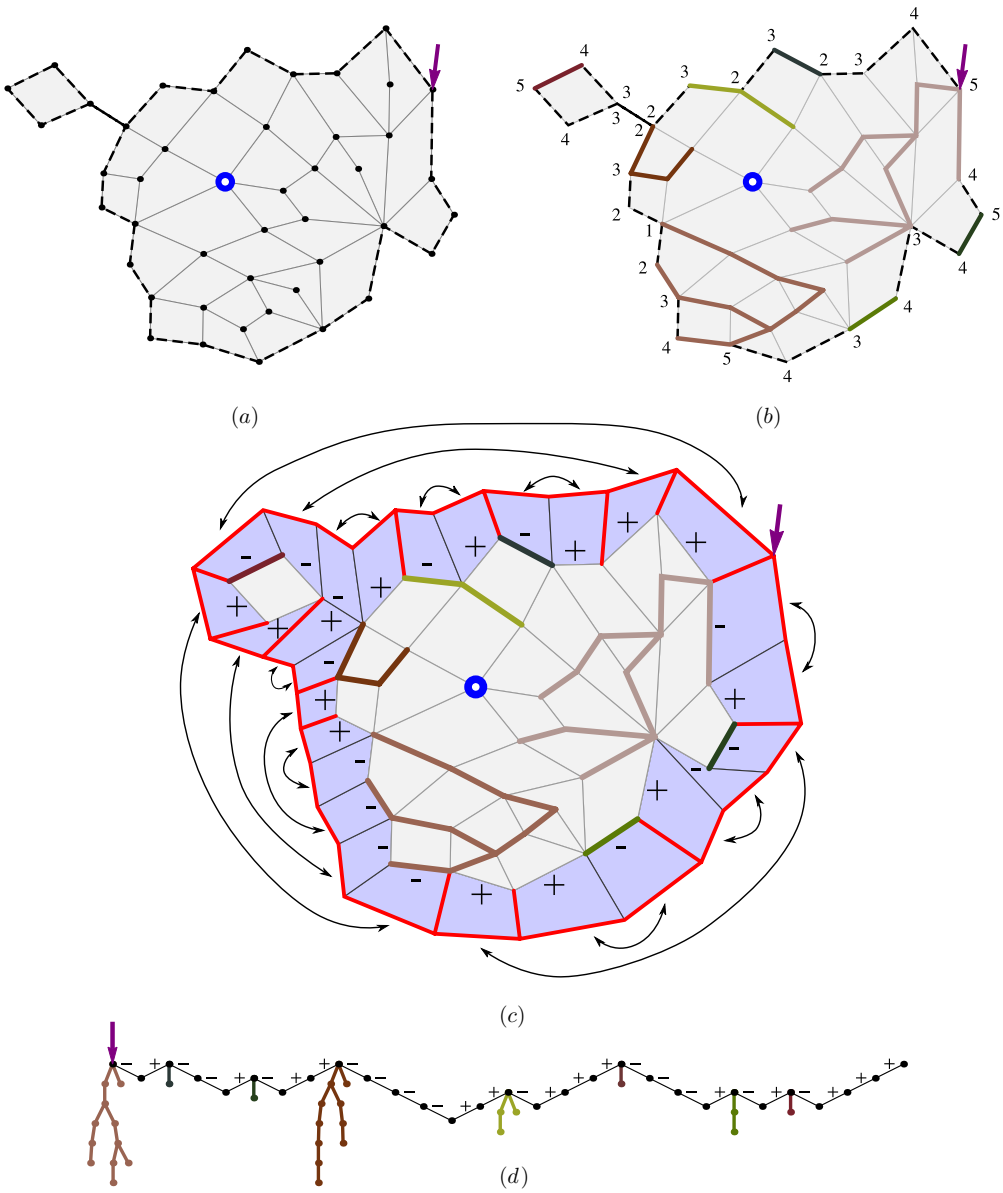

Figure 4. Quadrangulations with a boundary and an origin are in bijection with sequences of + and − with a (possibly empty) labeled planar tree growing from each end point of a +-edge.

mobiles. To keep the discussion self-contained, let us present here an alternative argument based on the Cori–Vauquelin–Schaeffer bijection alone.

We turn the quadrangulation with boundary into a quadrangulation of the 2-sphere by quadrangulating the boundary face, while making sure that the distance labeling is unaffected. A convenient method to do this is shown in figure 4(*c*). First an annulus consisting of $2l$ quadrangles is glued to the boundary. Notice that this does not change the distances from the original vertices to the origin and that the labels on the 'new boundary' are increased

by one compared to the 'old boundary'. Now we only have to find a pairwise gluing of the new boundary edges in such a way that only vertices with identical label are identified. A well-defined prescription is to repeatedly glue pairs consisting of a $-$-edge directly followed by a $+$-edge, until no boundary edges are left (see figure 4(*c*) for an example). Applying Schaeffer's prescription to the resulting pointed quadrangulation, we obtain a tree $\mathcal{T}$ which by construction contains the trees of $\mathcal{F}$ as subtrees. The complement $\mathcal{T} \setminus \mathcal{F}$ of $\mathcal{F}$ in $\mathcal{T}$, as shown in red in figure 4(*c*), is a tree arising from the coloring of the quadrangles in the annulus. The quadrangles adjacent to the $-$-edges provide the coloring of the whole new boundary (after the gluing). The quadrangles adjacent to the $+$-edges, on the other hand, lead to tree edges connecting the new boundary with all the ends of $+$-edges of the old boundary. Therefore only the ends of the $+$-edges are connected by the tree $\mathcal{T} \setminus \mathcal{F}$. Since $\mathcal{T}$ is connected and has no cycles, each tree of $\mathcal{F}$ must contain exactly one end of a $+$-edge.

One can root each tree of $\mathcal{F}$ at its distinguished vertex on the boundary by choosing the corner facing the external face. In order to turn them into rooted well-labeled trees, we may shift the labels on the trees by an integer such that each of them has minimal label equal to one, or, equivalently, we only keep track of the $+$ and $-$ along the edges of the trees. In general we may extract from a pointed quadrangulation rooted at its boundary of length $2l$ a sequence containing $l+$ and $l-$, representing the change in the labeling along the boundary, and l (possibly empty) rooted well-labeled trees which 'grow' from the end of the l $+$-edges (see figure 4(*d*)). It is not hard to see that one can reconstruct from this information the well-labeled tree $\mathcal{T}$ and therefore the full quadrangulation using the Cori–Vauquelin–Schaeffer bijection. A precise proof is given in [16, 20].

Using this bijection one can easily write down a generating function $w(g, l)$ for the number of pointed quadrangulations with N faces rooted on its boundary of length $2l$. Since we can arrange the $l+$ in any way along the boundary of length $2l$, we get

$$w(g, l) = \binom{2l}{l} z^{(\ell)}(g)^l, \tag{5}$$

where $z^{(\ell)}(g)$ is the generating function for labeled trees (2). In terms of the boundary cosmological constant y,

$$w(g, y) = \sum_{l=0}^{\infty} w(g, l) y^l = \frac{1}{\sqrt{1 - 4yz^{(\ell)}(g)}}. \tag{6}$$

To obtain the continuum disk function of 2D gravity we introduce a lattice spacing ϵ, in terms of which we can define a continuum volume $V = N\epsilon^2$ and boundary length $L = l\epsilon$ with canonical dimension. The Laplace transform $W_\Lambda(Y)$ of the continuum disk function $W_V(L)$ is obtained from the discrete disk function $w(g, y)$ by expanding around its critical point at $g_c = 1/12$, $y_c = 1/8$,

$$g = g_c(1 - \Lambda\epsilon^2), \quad y = y_c(1 - Y\epsilon). \tag{7}$$

Plugging these into (6), we obtain

$$w(g, y) = \frac{1}{\sqrt{Y + \sqrt{\Lambda}}} \epsilon^{-1/2}(1 + \mathcal{O}(\epsilon)) =: W^{\mathrm{m}}_\Lambda(Y)\epsilon^{-1/2}(1 + \mathcal{O}(\epsilon)), \tag{8}$$

where $W^{\mathrm{m}}_\Lambda(Y)$ is the continuum disk function with a marked point. The unmarked disk function (also known as the genus 0 sector of the Hartle–Hawking wave function of 2D gravity, see e.g. [2] section 4.4.2) is obtained by integrating W^{m}_Λ with respect to Λ (see also [20], section 4.4),

$$W_\Lambda(Y) = \frac{2}{3}\left(Y - \frac{1}{2}\sqrt{\Lambda}\right)\sqrt{Y + \sqrt{\Lambda}}. \tag{9}$$

More generally one can consider any ensemble of labeled trees with generating function $z(g)$ and compute the corresponding disk function. Provided that the ensemble has a susceptibility exponent $\gamma = 1/2$, i.e. $z(g)$ is of the form

$$z(g_c) - z(g) \propto (g_c - g)^{1/2}, \tag{10}$$

we can define the continuum tree amplitude Z through $z(g) = z(g_c)(1 - Z\epsilon + \mathcal{O}(\epsilon^2))$. The disk function is then simply

$$W^m(Y) = \frac{1}{\sqrt{Y+Z}}. \tag{11}$$

In particular, one can consider the generating function $z^{(u)}(g)$ for the ensemble of trees where all labels are $-$, related to the causal quadrangulations. The continuum amplitude is simply $Z^{(u)} = \sqrt{\Lambda}$, which is exactly the same as for the labeled trees. In contrast to what one might have expected, restricting to causal quadrangulations does not change the continuum disk function.

The explanation is that this particular disk function is not the one usually considered in the context of CDT. To recover the latter one should consider the disk function where the boundary is restricted to be at constant distance from the origin. In terms of the quadrangulations this is achieved by restricting the labels on the boundary to alternate between two consecutive integers, or, using the bijection, by fixing the boundary sequence to $(+, -, +, -, +, \ldots)$. Since there is only one such sequence, we lose the combinatorial factor in (5) and end up with the disk function

$$w_c(g, y) = \sum_{l=0}^{\infty} w(g, l) y^l = \frac{1}{1 - y\, z(g)}. \tag{12}$$

Its continuum counterpart is

$$W^c_\Lambda(Y) = \frac{1}{Y+Z}, \tag{13}$$

which differs from the unrestricted disk function (11) only by an overall square root. We reproduce the standard CDT disk function[4] by setting $Z = \sqrt{\Lambda}$.

Notice that the overall square root in the marked DT disk function $W^m_\Lambda(Y)$ compared to the CDT disk function $W^c_\Lambda(Y)$ is simply a consequence of the labeling describing a random walk on the boundary. As we will see in section 4, only once the random character of the labeling on the trees is taken into account, will the stark difference in scaling of DT compared to CDT be revealed.

In the next section we will introduce a new partition function for labeled trees, to which we can assign disk functions like above.

3. From quadrangulations to generalized CDT

As mentioned earlier causal quadrangulations are characterized by a single local maximum of the labeling, while general quadrangulations can have any number. This suggests a convenient way to interpolate between both models, by assigning a coupling $\mathfrak{g}$ to each local maximum. Then by construction setting $\mathfrak{g} = 0$ will lead to a model of closed causal quadrangulations and $\mathfrak{g} = 1$ to general quadrangulations. If we interpret the labeling as a time function, we can also

[4] To get the exact generating function for causal triangulations, one has to glue triangles to all $(-, +)$ pairs on the boundary. The generating function $w_{\rm CDT}(g, y)$ for the number of causal triangulations with a fixed number of triangles and a fixed boundary length is then $w_{\rm CDT}(g, y) = w_c(g^2, gy)$.

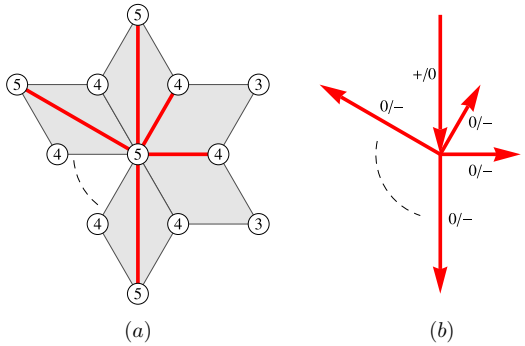

Figure 5. A local maximum on the quadrangulation corresponds to a local maximum on the tree, i.e. to a vertex with a +- or 0-edge coming in and all outgoing edges carrying a 0 or a −.

view the coupling $\mathfrak{g}$ as a weight for the process of a universe splitting in two, i.e. of spatial topology change.

A model of spatial topology change in continuum CDT was studied in [9–11] and was referred to as *generalized CDT*. To prevent a proliferation of baby universes in the continuum limit it was found that the coupling $\mathfrak{g}$ should be scaled to zero with the lattice spacing ϵ as $\mathfrak{g} = \mathfrak{g}_s\epsilon^3$. The continuum disk function could be calculated from a graphical consistency relation, leading to

$$W_{\lambda,\mathfrak{g}_s}(X) = \frac{-(X^2-\lambda) + (X-\alpha)\sqrt{(X+\alpha)^2 - 2\mathfrak{g}_s/\alpha}}{2\mathfrak{g}_s}, \tag{14}$$

where λ is the 'effective' CDT cosmological constant (to be discussed in more detail below equation (22)) and $\alpha = \alpha(\mathfrak{g}_s, \lambda)$ is given by the (largest) solution to

$$\alpha^3 - \lambda\alpha + \mathfrak{g}_s = 0. \tag{15}$$

This equation ensures that $XW_{\lambda,\mathfrak{g}_s}(X) \to 1$ for $X \to \infty$. In the following we will show how we can derive $W_{\lambda,\mathfrak{g}_s}(X)$ by counting quadrangulations with a weight assigned to the local maxima of their labeling and then taking a suitable continuum limit.

However, before we continue, let us introduce a more convenient version of the disk amplitude in (14), for which one of the end points of the baby universes, i.e. one of the local maxima of the time function, is marked. The term of order $\mathfrak{g}_s^n$ in (14) corresponds to surfaces with $n+1$ such local maxima. Hence we introduce the *cap function*

$$W^{\mathrm{cap}}_{\lambda,\mathfrak{g}_s}(X) = \frac{1}{\sqrt{(X+\alpha)^2 - 2\mathfrak{g}_s/\alpha}}, \tag{16}$$

which satisfies

$$W^{\mathrm{cap}}_{\lambda,\mathfrak{g}_s}(X) = \frac{\partial}{\partial\mathfrak{g}_s}(\mathfrak{g}_s W_{\lambda,\mathfrak{g}_s}(X)), \tag{17}$$

where the derivative is taken while keeping X and λ fixed.

A vertex with label t is a local maximum on the quadrangulation if all its neighbors, i.e. the vertices connected to it by an edge of the quadrangulation, are labeled $t-1$, as in figure 5(*a*). Equivalently, its neighbors in the associated well-labeled tree are labeled by t or $t-1$. Therefore, in terms of the rooted labeled trees we should associate a coupling $\mathfrak{g}$ to every vertex in the tree which has a +- or 0-edge coming in (or no edge in the case of the root vertex) and all outgoing edges carrying a 0 or a − (figure 5(*b*)). Let us denote by $z_0(g) = z_0(g, \mathfrak{g})$ the generating function for such trees. Similarly we introduce the generating

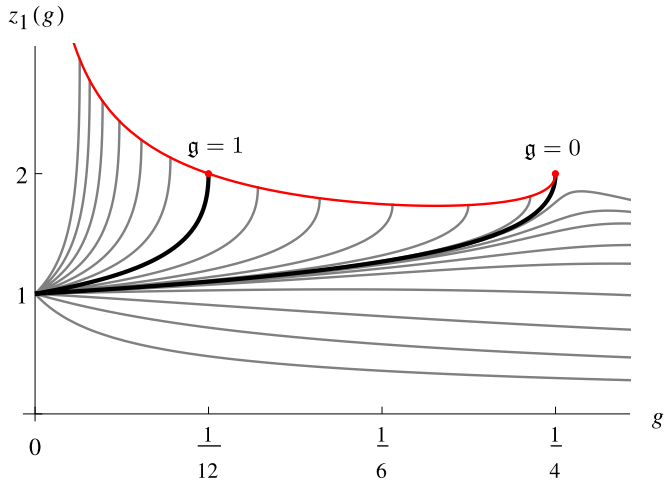

Figure 6. The solution of equation (19) for various values of $\mathfrak{g}$ as a function of g. For each value of $\mathfrak{g} \leqslant 0$ the curve ends at the critical line, defined by equation (20).

function $z_1(g) = z_1(g, \mathfrak{g})$ with the only difference that we do not assign a coupling $\mathfrak{g}$ to the root vertex, even if there is local maximum there. Both $z_0(g)$ and $z_1(g)$ therefore reduce to the generating function for rooted well-labeled trees $z^{(\ell)}(g)$ from (2) in the case $\mathfrak{g} = 1$. We obtain recurrence relations for $z_0(g)$ and $z_1(g)$ by summing over the number and associated labels of the edges leaving the root,

$$\begin{aligned} z_1 &= \sum_{k=0}^{\infty} (gz_1 + gz_0 + gz_0)^k = \frac{1}{1 - gz_1 - 2gz_0} \\ z_0 &= \sum_{k=0}^{\infty} (gz_1 + gz_0 + gz_0)^k + (\mathfrak{g} - 1) \sum_{k=0}^{\infty} (gz_1 + gz_0)^k \\ &= z_1 + \frac{(\mathfrak{g} - 1)}{1 - gz_1 - gz_0}. \end{aligned} \tag{18}$$

These combine into a single fourth-order polynomial for $z_1(g)$,

$$3g^2 z_1^4 - 4g z_1^3 + (1 + 2g(1 - 2\mathfrak{g}))z_1^2 - 1 = 0. \tag{19}$$

The relevant solution, i.e. the one of the form $z_1(g) = 1 + \mathcal{O}(g)$, is given by its smallest positive root. For $\mathfrak{g} = 1$ the solution reduces to (2), while for $\mathfrak{g} = 0$ we get the generating function for unlabeled trees (4), $z_1(g)|_{\mathfrak{g}=0} = z^{(u)}(g)$. The latter is not true for $z_0(g)$ since each labeled tree must have at least one local maximum, hence $z_0(g) = 0$ for $\mathfrak{g} = 0$.

In figure 6 we have plotted the solutions for various other fixed values of $\mathfrak{g}$. For each $\mathfrak{g} \geqslant 0$ there is a critical value $g_c(\mathfrak{g})$ at which $z_1(g)$ becomes non-analytic and at which a continuum limit can be taken. This critical value $g_c(\mathfrak{g})$ is determined by the additional requirement that the derivative $z_1'(g)$ of $z_1(g)$ diverges, which leads to the equation

$$3g_c^2 z_1^4 - 2g_c z_1^3 + 1 = 0. \tag{20}$$

This curve is plotted in red in figure 6.

Unless $\mathfrak{g} = 0$ we obtain an infinite density of baby universes in the continuum limit and presumably we end up in the same universality class as pure DT. This can be seen by

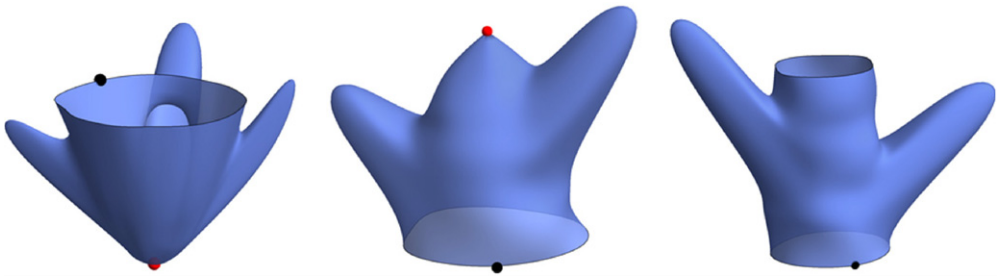

Figure 7. (*a*) The cup function $W^{\rm cup}_{\lambda,\mathfrak{g}_s}(Y)$, (*b*) the cap function $W^{\rm cap}_{\lambda,\mathfrak{g}_s}(X)$ and (*c*) the propagator $G_{\lambda,\mathfrak{g}_s}(X,Y;T)$.

calculating the expected number $\langle N_{\rm max}(\mathfrak{g})\rangle_N$ of local maxima for fixed large number N of faces, which satisfies

$$\langle N_{\rm max}(\mathfrak{g})\rangle_N = \rho(\mathfrak{g})N + \mathcal{O}(N^0), \quad \rho(\mathfrak{g}) = 2\left(\frac{\mathfrak{g}}{2}\right)^{2/3} + \mathcal{O}(\mathfrak{g}), \quad \rho(1) = \frac{1}{2}. \tag{21}$$

If we want to keep $\langle N_{\rm max}(\mathfrak{g})\rangle_N$ finite as $N \to \infty$ we should instead scale $\mathfrak{g}$ to zero like $N^{-3/2}$. In the grand-canonical setting this corresponds to scaling $\mathfrak{g} = \mathfrak{g}_s\epsilon^3$ with the lattice spacing ϵ, as observed previously. To take this continuum limit we again expand g around its critical value $g_c(\mathfrak{g}) = 1/4 - 3/4(\mathfrak{g}/2)^{2/3} + \mathcal{O}(\mathfrak{g})$,

$$g = g_c(\mathfrak{g})(1-\Lambda\epsilon^2) = \frac{1}{4}\left(1 - 3\left(\frac{\mathfrak{g}_s}{2}\right)^{2/3}\epsilon^2 - \Lambda\epsilon^2\right) = \frac{1}{4}(1-\lambda\epsilon^2), \tag{22}$$

where $\lambda = \Lambda + 3\left(\frac{\mathfrak{g}_s}{2}\right)^{2/3}$ is the 'effective' cosmological constant as was introduced originally in generalized CDT [11]. The original model was formulated directly in the continuum limit and only later, using matrix models, was it understood that λ is actually a sum of contributions coming from a 'genuine' cosmological constant Λ related to the 'area' of graphs (triangulations, quadrangulations etc.) and a (string) coupling constant $\mathfrak{g}_s$ from splitting off baby universes [3].

Plugging (22) and $z_1(g) = z_1(g_c)(1 - Z_1\epsilon)$ into (19) we obtain the continuum equation

$$Z_1^3 - \lambda Z_1 + \mathfrak{g}_s = 0. \tag{23}$$

Notice that this is exactly equation (15) with $\alpha = Z_1$.

According to (13) the disk function with constant distance to the origin associated to this ensemble of labeled trees is given by

$$W^{\rm cup}_{\lambda,\mathfrak{g}_s}(Y) = \frac{1}{Y + Z_1}, \tag{24}$$

which is different from (16). The difference is in the distance function used for the labeling. Here the labeling corresponds to the distance to the marked origin in the disk, while in (16) the distance to the boundary is used and one of the local maxima of the time function is marked. We refer to these two disk functions as the *cup function* $W^{\rm cup}_{\lambda,\mathfrak{g}_s}(Y)$ and the *cap function* $W^{\rm cap}_{\lambda,\mathfrak{g}_s}(X)$, see figure 7. In order to obtain the cap function we will now study more general time-dependent amplitudes, in particular the two-loop propagator $G_{\lambda,\mathfrak{g}_s}(X,Y;T)$ (figure 7(*c*)) and the two-point function $G_{\lambda,\mathfrak{g}_s}(T)$.

4. Time-dependent amplitudes

The simple generating functions discussed in the previous section provide little information about the geometry of the quadrangulations they encode. In order to better understand the geometries and to fully reproduce the results of [11] we need to keep track of the labeling on the trees in more detail. Let us define the generating function $z_0(t) = z_0(t, g, \mathfrak{g})$ for rooted trees with positive integer labels on its vertices, such that the labels differ by at most one along the edges and such that the root is labeled t. Then $z_0(t) - z_0(t-1)$ is the generating function for rooted well-labeled trees, i.e. labeled trees with minimal label equal to 1, with root labeled t. According to the bijections in section 2, $z_0(t)$ also gives a generating function for the quadrangulations of the sphere with the furthest end point of its root edge at most a distance t from the origin, again including a factor of $\mathfrak{g}$ for each local maximum of the distance functions. Likewise, the generating function where this distance is exactly t is $z_0(t) - z_0(t-1)$.

As in the previous section we introduce $z_1(t) = z_1(t, g, \mathfrak{g})$ for which no coupling $\mathfrak{g}$ is assigned to the root vertex. The recurrence relations (18) straightforwardly generalize to

$$\begin{aligned} z_1(t) &= \frac{1}{1 - g\, z_1(t-1) - g\, z_0(t) - g\, z_0(t+1)}, \\ z_0(t) &= z_1(t) + \frac{(\mathfrak{g}-1)}{1 - g\, z_1(t-1) - g\, z_0(t)} \end{aligned} \tag{25}$$

for $t \geqslant 1$, subject to the boundary conditions $z_1(0) = 0$ and $z_0(\infty) = z_0$.

Quite remarkably, (25) can be solved analytically using the technique outlined in [17, 24]. Expanding the generating functions around their limits as $t \to \infty$, which are given by the solution z_1 and z_0 to (18), we find after a straightforward but tedious calculation

$$\begin{aligned} z_1(t) &= z_1 \frac{1-\sigma^t}{1-\sigma^{t+1}} \frac{1-(1-\beta)\sigma - \beta\sigma^{t+3}}{1-(1-\beta)\sigma - \beta\sigma^{t+2}}, \\ z_0(t) &= z_0 \frac{1-\sigma^t}{1-(1-\beta)\sigma - \beta\sigma^{t+1}} \frac{(1-(1-\beta)\sigma)^2 - \beta^2\sigma^{t+3}}{1-(1-\beta)\sigma - \beta\sigma^{t+2}}, \end{aligned} \tag{26}$$

where β and σ are fixed in terms of z_0 and z_1 (hence in terms of g and $\mathfrak{g}$) through

$$\begin{aligned} g(1+\sigma)(1+\beta\sigma)z_1 - \sigma(1-2g\, z_0) &= 0, \\ (1-\beta)\sigma - g(1+\sigma)z_1 + g(1-\sigma+2\beta\sigma)z_0 &= 0. \end{aligned} \tag{27}$$

In particular, $\beta = 0$ in the case of CDT ($\mathfrak{g} = 0$) and $\beta = 1$ in the case of DT ($\mathfrak{g} = 1$).

To get to generalized CDT in the continuum limit, the time should be scaled canonically with the lattice spacing, i.e. $t = T/\epsilon$. The scaling $\mathfrak{g} = \mathfrak{g}_s\epsilon^3$ and $g = 1/4(1-\lambda\epsilon^2)$ implies that the parameters σ and β scale as $\sigma = 1 - 2\Sigma\epsilon$ and $\beta = B\epsilon$. According to (27) the continuum parameters Σ and B are related to λ and $\mathfrak{g}_s$ through

$$\begin{aligned} \mathfrak{g}_s - 2B(B^2 + 3B\Sigma + 2\Sigma^2) &= 0, \\ \lambda - 3B^2 - 6B\Sigma - \Sigma^2 &= 0. \end{aligned} \tag{28}$$

They can also be expressed in terms of $\mathfrak{g}_s$ and α from equation (15),

$$\begin{aligned} \Sigma &= \frac{1}{2}\sqrt{4\alpha^2 - 2\mathfrak{g}_s/\alpha} \quad \left(= \sqrt{\lambda} - \frac{3\mathfrak{g}_s}{4\lambda} + \mathcal{O}\big(\mathfrak{g}_s^2\big)\right), \\ B &= \alpha - \Sigma. \end{aligned} \tag{29}$$

We also note that, as $\mathfrak{g}_s \to \infty$, α and Σ grow as

$$\alpha = \left(\frac{\mathfrak{g}_s}{2}\right)^{1/3} + \left(\frac{\Lambda}{3}\right)^{1/2} + O\left(\mathfrak{g}_s^{-1/3}\right), \quad \Sigma = (3\Lambda)^{1/4}\left(\frac{\mathfrak{g}_s}{2}\right)^{1/6} + O\left(\mathfrak{g}_s^{-1/6}\right). \tag{30}$$

Finally, the solutions (26) scale as $z_1(t) = 2(1 - Z_1(T)\epsilon)$ and $z_0(t) = 2Z_0(T)\epsilon^2$ with

$$Z_1(T) = \alpha + \frac{\Sigma^2}{\sinh(\Sigma T)\,[\Sigma\cosh(\Sigma T) + \alpha\sinh(\Sigma T)]},$$
$$Z_0(T) = \frac{\mathfrak{g}_s}{2\alpha}\left(1 - \frac{\Sigma^2}{[\Sigma\cosh(\Sigma T) + \alpha\sinh(\Sigma T)]^2}\right). \tag{31}$$

Since $z_0(t) - z_0(t-1)$ defines a discrete two-point function, the scaling limit of the two-point function is obtained by differentiating $Z_0(T)$ with respect to T,

$$G_{\lambda,\mathfrak{g}_s}(T) = \frac{\mathrm{d}Z_0(T)}{\mathrm{d}T} = \Sigma^3\,\frac{\mathfrak{g}_s}{\alpha}\,\frac{\Sigma\sinh\Sigma T + \alpha\cosh\Sigma T}{(\Sigma\cosh\Sigma T + \alpha\sinh\Sigma T)^3}. \tag{32}$$

In the limit $\mathfrak{g}_s \to 0$ we obtain (up to a factor $\mathfrak{g}_s$ which is convention) the CDT result

$$G_{\lambda,\mathfrak{g}_s=0}(T) \sim \mathrm{e}^{-2\sqrt{\Lambda}T}. \tag{33}$$

In the limit $\mathfrak{g}_s \to \infty$ we obtain (again up to a $\mathfrak{g}_s$ factor)

$$G_{\lambda,\mathfrak{g}_s\to\infty}(T) \sim \Lambda^{3/4}\frac{\cosh(\Lambda^{1/4}T')}{(\sinh(\Lambda^{1/4}T'))^3}, \quad T' = 3^{1/4}\left(\frac{\mathfrak{g}_s}{2}\right)^{1/6}T. \tag{34}$$

Of course this limit does not exist unless we keep T' finite in the scaling limit rather than T. Thus we are really discussing another scaling limit! Recall that $T \sim t/\epsilon$ and $\mathfrak{g}_s = \mathfrak{g}/\epsilon^3$. Thus a finite T' in the limit $\epsilon \to 0$ can be identified with a scaling limit where $t/\epsilon^{1/2}$ is finite for $\epsilon \to 0$. This is precisely the limit first discussed by Kawai *et al* [30] where the *geodesic* distance scales anomalously with respect to volume, leading to the Hausdorff dimension $d_h = 4$ for 2D Euclidean quantum gravity and in the DT ensemble of random graphs. The two-point function (34) was first calculated in [12] (see also [7] and [13] for more general formulas). We note that the 'DT limit' $\mathfrak{g}_s \to \infty$ can be identified with the limit $\lambda/(\mathfrak{g}_s/2)^{2/3} \to 3$ from above and is the limit where equation (23) ceases to have a real positive solution Z_1.

4.1. The disk functions and propagator

Let us now turn to surfaces with one or more boundary components. We will first present a heuristic derivation of the disk function $W_{\lambda,\mathfrak{g}_s}(X)$ in (14) using only the continuum tree amplitudes $Z_0(T)$ and $Z_1(T)$. Below we will see that $W_{\lambda,\mathfrak{g}_s}(X)$ can also be obtained directly in the scaling limit of quadrangulations with a boundary, by relating it to the propagator with a final boundary of length 0.

The cup function $(Y + Z_1(T))^{-1}$ constructed from $Z_1(T)$ corresponds to a path integral over all surfaces with a boundary at constant distance smaller than T from the origin. The corresponding cup function for fixed boundary length L is its inverse Laplace transform and equals

$$\mathrm{e}^{-LZ_1(T)}. \tag{35}$$

We note that this function can be used to reveal a relation between $Z_0(T)$, $Z_1(T)$ and the disk function $W_{\lambda,\mathfrak{g}_s}(X)$ (which is the cap function without a mark in (14) and which we will determine by combinatorial methods below). In figure 8 we have depicted the two-point function $Z_0(T)$, which is a path integral over surfaces with two marked points, i.e. the origin and the root, separated by a distance smaller than T. This two-point function can be decomposed as follows: first one moves from the origin to the root at a distance $T' \leqslant T$ from the origin. This root is located on a connected curve of some length L where all points have the same distance T' to the origin. Cutting the surface along this curve leads to two disks, both with a mark on the boundary. The bottom disk (see figure 8) has an origin at a fixed distance $T' \leqslant T$ from the boundary and therefore its amplitude is given by (35). The top disk has no mark in its

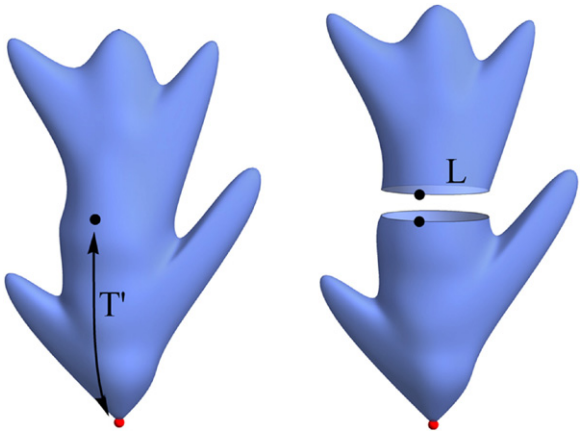

Figure 8. The two-point function $Z_0(T)$ can be obtained by 'closing off' the boundary of a cup function at a fixed distance $T' < T$ from the origin by the disk amplitude.

interior and the labeling is determined by the distance to the boundary of length L, hence its amplitude corresponds to the inverse Laplace transform $\tilde{W}_{\lambda,\mathfrak{g}_s}(L)$ of the disk function $W_{\lambda,\mathfrak{g}_s}(X)$. The two-point function $Z_0(T)$ is therefore obtained by combining these to disk amplitudes and integrating over L, i.e.

$$Z_0(T) = \mathfrak{g}_s \int_0^\infty \mathrm{d}L\, \tilde{W}_{\lambda,\mathfrak{g}_s}(L)\, \mathrm{e}^{-LZ_1(T)} = \mathfrak{g}_s W_{\lambda,\mathfrak{g}_s}(Z_1(T)). \tag{36}$$

We have to include a factor of $\mathfrak{g}_s$ simply because $Z_0(T)$ has a coupling $\mathfrak{g}_s$ for each local maximum, while the term of order $\mathfrak{g}_s^n$ in the disk function $W_{\lambda,\mathfrak{g}_s}(X)$ corresponds to surfaces with $n+1$ local maxima (see the discussion above equation (16)). Since we have explicitly determined $Z_0(T)$ and $Z_1(T)$ we can verify using (36) that $W_{\lambda,\mathfrak{g}_s}(X)$ is indeed given by formula (14).

The *propagator* $G_{\lambda,\mathfrak{g}_s}(X, Y; T)$ corresponds to the path integral over surfaces with two boundaries, an initial boundary with boundary cosmological constant X and a final boundary at a fixed distance T from the initial boundary with boundary cosmological constant Y (see figure 7(*c*)). In order to find an expression for $G_{\lambda,\mathfrak{g}_s}(X, Y; T)$ in the scaling limit of generalized CDT a suitable ensemble of quadrangulations has to be chosen. Let us define $\mathcal{Q}_{l_1,l_2,t}(N)$, $t \geqslant 1$, to be the set of quadrangulations Q with N quadrangles and two boundaries, the 'initial' and 'final' boundary, of lengths[5] $2l_1$ and $2l_2$, rooted at the final boundary and satisfying the following conditions. First of all we require that the initial boundary is *non-degenerate* in the sense that all the corners of the boundary face belong to distinct vertices. In order to state the second requirement a canonical labeling of the vertices is introduced. If t is odd, the vertices on the initial boundary that have even distance to the root are labeled 0. Otherwise the vertices with odd distance are labeled 0. All remaining vertices are labeled by their minimal distance to the set of vertices labeled 0. Given this canonical labeling, the vertices on the final boundary are required to have label t or $t+1$, which is a discrete implementation of the fixed distance between the boundaries which we are after in the continuum. An example of a quadrangulation in $\mathcal{Q}_{l_1,l_2,t}(N)$ with $N = 56$, $l_1 = 5$, $l_2 = 13$ and $t = 3$ is shown in figure 9(*a*).

[5] Even though quadrangulations with two boundaries of *odd* length exist, we require the boundary lengths to be even to keep them bipartite.

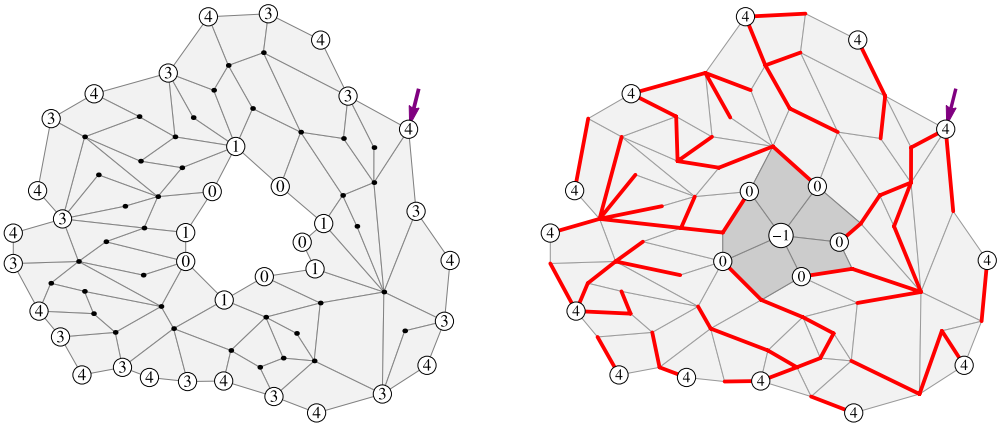

(*a*) (*b*)

Figure 9. (*a*) A quadrangulation with two boundaries contributing to the discrete propagator. (*b*) The initial boundary face can be quadrangulated by inserting a new vertex with label -1, turning the quadrangulation into a pointed quadrangulation with a single boundary.

We can close off the initial boundary by gluing to it a disk constructed from l_1 simple faces, i.e. each of them labeled $(-1, 0, 1, 0)$ (see figure 9(*b*)). This way we obtain a pointed quadrangulation, for which the origin is labeled -1 instead of the usual 0, with a single boundary. According to the bijection discussed in section 2.4 (and taking into account an overall shift of the labels by -1), this quadrangulation can be encoded by a forest of l_2 rooted trees, one 'growing' from each vertex labeled $t+1$ on the final boundary (see figure 9(*b*)). The vertices of the trees carry non-negative labels, differing by at most one along the edges and having label $t+1$ on the root. The quadrangulations under consideration have a special structure at the origin, namely that all l_1 faces around the origin are simple and that the l_1 edges starting at the origin end at distinct vertices. In terms of the rooted trees with their edges directed away from the root, this condition translates exactly into the condition that the vertices labeled 0 have no outgoing edges. The number of vertices labeled 0 in the whole forest is l_1.

In order to count these quadrangulations we introduce the generating functions $z_{i,x}(t) = z_{i,x}(t, g, \mathfrak{g})$, $i = 0, 1$, for rooted trees labeled by non-negative integers which differ by at most one along the edges, having label t on the root, no edges starting at a vertex labeled 0, carrying a factor of x/g for each vertex labeled 0 and a factor of $\mathfrak{g}$ for each local maximum (except for the one at the origin in the case of $z_{1,x}(t)$). When $x = 0$ the labels are restricted to be positive and therefore $z_{i,x=0}(t) = z_i(t)$, where $z_i(t)$ are the generating functions from before. It is not hard to see that for $x > 0$ the $z_{i,x}(t)$ satisfy exactly the same equations (25) but with the boundary condition $z_{1,x}(0) = x/g$ instead of $z_1(0) = 0$.

The generating function $\mathcal{G}_{\mathfrak{g}}(x, y, g; t)$ for the number of quadrangulations in $\mathcal{Q}_{l_1,l_2,t}(N)$, including a factor $\mathfrak{g}$ for each local maximum away from the final boundary, is then given by

$$\begin{aligned}\mathcal{G}_{\mathfrak{g}}(x, y, g; t) &= \sum_{l_1=1}^{\infty}\sum_{l_2=1}^{\infty}\sum_{N=0}^{\infty} x^{l_1} y^{l_2} g^N \sum_{Q\in\mathcal{Q}_{l_1,l_2,t}(N)} \mathfrak{g}^{N_{\max}(Q)} \\ &= \sum_{l_2=1}^{\infty} y^{l_2}[(z_{1,x}(t+1))^{l_2} - (z_1(t+1))^{l_2}], \end{aligned} \tag{37}$$

where the x-independent part $(z_1(t+1))^{l_2}$ has been subtracted on the right-hand to ensure $l_1 \geqslant 1$.

Since the solution (26) solves (25) for any *real* value $t > 0$ and $z_1(t)$ increases monotonically from 0 at $t = 0$ to z_1 at $t \to \infty$, we find (with a slight abuse of notation)

$$z_{1,x}(t) = z_1\left(t + z_1^{-1}(x/g)\right), \tag{38}$$

provided $0 \leqslant x/g < z_1$. This solution has a critical point at $x = gz_1$, around which $z_{1,x}(t)$ should be expanded to get the canonical scaling of the initial boundary length in the continuum limit. Setting $x = 1/2(1 - X\epsilon + \mathcal{O}(\epsilon^2))$ leads to $z_{1,x}(t) = 2(1 - Z_{1,X}(T)\epsilon + \mathcal{O}(\epsilon^2))$ with

$$Z_{1,X}(T) = Z_1(T + Z_1^{-1}(X)). \tag{39}$$

However, one has to keep in mind that this solution is only valid for $X > Z_1 = \alpha$. To get the other part of the solution we have to solve (25) with $\bar{z}_1(t) > z_1$, which can be formally obtained by shifting $t \to t + \mathrm{i}\pi/(\log\sigma)$. The corresponding continuum solution $\bar{Z}_1(T)$ is obtained from (31) by shifting $T \to T - \mathrm{i}\pi/(2\Sigma)$. This $\bar{Z}_1(T)$ grows monotonically from $\sqrt{2\mathfrak{g}_s/\alpha} - \alpha$ to α and therefore allows us to construct $Z_{1,X}(T)$ for $\sqrt{2\mathfrak{g}_s/\alpha} - \alpha < X < \alpha$. Notice that $X > \sqrt{2\mathfrak{g}_s/\alpha} - \alpha$ is exactly the region where (16) is real and non-singular.

If in addition the final boundary cosmological constant is scaled as $y = 1/2(1 - Y\epsilon + \mathcal{O}(\epsilon^2))$, it follows from (37) that

$$\mathcal{G}_{\mathfrak{g}}(x, y, g; t) = \left(\frac{1}{Y + Z_{1,X}(T)} - \frac{1}{Y + Z_1(T)}\right)\epsilon^{-1} + \mathcal{O}(\epsilon^0). \tag{40}$$

The term in the parentheses is almost the sought-after propagator $G_{\lambda,\mathfrak{g}_s}(X, Y; T)$, except that the final boundary is marked, while we want only the initial boundary to be marked (see figure 7(*c*)). To get $G_{\lambda,\mathfrak{g}_s}(X, Y; T)$ a factor of l_1/l_2 should be included in the sum (37), or, equivalently, one can differentiate (40) with respect to X and integrate with respect to Y,

$$G_{\lambda,\mathfrak{g}_s}(X, Y; T) = \int_\infty^Y \mathrm{d}Y' \frac{\partial}{\partial X}\left(\frac{1}{Y' + Z_{1,X}(T)}\right) = \frac{Z'_{1,X}(T)}{Z'_{1,X}(0)}\frac{1}{Y + Z_{1,X}(T)}. \tag{41}$$

The cap function is obtained from the propagator by integrating over T and taking the final boundary length to zero,

$$W^{\mathrm{cap}}_{\lambda,\mathfrak{g}_s}(X) = \lim_{Y\to\infty} Y \int_0^\infty \mathrm{d}T\, G_{\lambda,\mathfrak{g}_s}(X, Y; T) = \frac{Z_1 - X}{Z'_1(Z_1^{-1}(X))}. \tag{42}$$

From (31) it follows that

$$Z'_{1,X}(T) = (\alpha - Z_{1,X}(T))\sqrt{(Z_{1,X}(T) + \alpha)^2 - 2\mathfrak{g}_s/\alpha} =: -\bar{W}(Z_{1,X}(T)), \tag{43}$$

where we have introduced the notation

$$\bar{W}(X) = (X - \alpha)\sqrt{(X + \alpha)^2 - 2\mathfrak{g}_s/\alpha}, \tag{44}$$

and thus (42) reproduces exactly (16). Further, (41) shows that the loop propagator satisfies the differential equation

$$\frac{\partial}{\partial T} G_{\lambda,\mathfrak{g}_s}(X, Y; T) = -\frac{\partial}{\partial X}(\bar{W}(X) G_{\lambda,\mathfrak{g}_s}(X, Y; T)), \tag{45}$$

since (43) is the characteristic equation for (45) and (41) is thus the solution with initial boundary condition

$$G_{\lambda,\mathfrak{g}_s}(X, Y; T = 0) = \frac{1}{X + Y}, \quad \text{or} \quad \tilde{G}_{\lambda,\mathfrak{g}_s}(L_1, L_2; T = 0) = \delta(L_1 - L_2), \tag{46}$$

where $\tilde{G}_{\lambda,\mathfrak{g}_s}(L_1, L_2; T)$ is the inverse Laplace transform of $G_{\lambda,\mathfrak{g}_s}(X, Y; T)$.

An alternative route toward the solutions (31) and the propagator (41) is to directly take the continuum limit of the recurrence relations (25). This is done by substituting

$$\begin{aligned} z_1(t+s) &= 2\left(1+\epsilon(Z_1(T)+s\,\epsilon Z_1'(T))\right) \\ z_0(t+s) &= 2\epsilon^2\left(Z_0(T)+s\,\epsilon Z_0'(T)\right) \end{aligned} \qquad s\in\{0,1,2,3\}, \tag{47}$$

in (25) leading to the differential equations

$$Z_1'(T) = \lambda - Z_1(T)^2 - 2Z_0(T), \tag{48}$$

$$Z_0'(T) = 2Z_1(T)Z_0(T) - \mathfrak{g}_s. \tag{49}$$

It can be checked that these equations are solved by (31), but it might be more enlightening to show how they contain all information about the disk function. First we note that the equations imply

$$Z_1''(T) = 2(Z_1(T)^3 - \lambda Z_1(T) + \mathfrak{g}_s). \tag{50}$$

Integration and the assumption that $Z_1(T)\to Z_1=\alpha$ for $T\to\infty$ then implies:

$$Z_1'(T) = -\bar{W}(Z_1(T)),\, Z_0(T) = \mathfrak{g}_s W_{\lambda,\mathfrak{g}_s}(Z_1(T)), \tag{51}$$

where $W_{\lambda,\mathfrak{g}_s}(X)$ is given by (14). While this determines $W_{\lambda,\mathfrak{g}_s}(X)$ algebraically, one has to appeal to figure 8, say, to identify it as the disk function, as done previously.

5. Generalized CDT in terms of general planar maps

Above we have seen that pointed quadrangulations with a certain number of local maxima of the distance functions can be encoded in well-labeled planar trees with the same number of local maxima. As we will demonstrate in this section, a set of planar maps including faces of any degree can be used to encode the same information.

There exists a well-known bijection Φ_0, often referred to as the *trivial bijection* (see e.g. [34]), between pointed quadrangulations with N faces and pointed planar maps with N edges. It can be formulated in a very similar way as the Cori–Vauquelin–Schaeffer bijection, namely in terms of the distance labeling from the origin. Instead of applying the Schaeffer prescription in figure 1(*a*), for each face the diagonal is drawn that connects vertices of even label. In this way all vertices with even label will be part of the planar map, and the vertices with odd label are in one-to-one correspondence with the faces of the map. It can be seen that this planar map with marked origin completely characterizes the quadrangulation.

However, as we will see below, there exists another inequivalent bijection between rooted pointed quadrangulations Q with N faces and rooted pointed planar maps with N edges. Although we expect this bijection to be known, since it is quite similar to the bijection introduced by Miermont in [36] and used in [19], we were unable to find an explicit reference to it in the literature. The bijection is a consequence of the general result in theorem 1 below, which is quite similar to theorem 4 in [36]. To keep the discussion self-contained we provide a proof, which is largely inspired by the proofs in [22, 36].

Let $\mathcal{Q}^{(l)}$ be the set of rooted quadrangulations of the sphere, i.e. quadrangulations with a marked unoriented edge, equipped with integer labels on the vertices, such that the labels differ by exactly one along the edges. Let $\mathcal{M}^{(l)}$ be the set of rooted planar maps with integer labels on the vertices, such that the labels differ by *at most* one along the edges. Given a labeled rooted quadrangulation $Q\in\mathcal{Q}^{(l)}$, according to lemma 1, application of Schaeffer's prescription leads to a planar map. This planar map is naturally labeled, since its vertices are also vertices of Q, and it can be rooted at the corner containing the end point with largest label of the root edge of Q. Hence, one obtains a labeled rooted planar map, which we denote by $\Psi(Q)\in\mathcal{M}^{(l)}$.

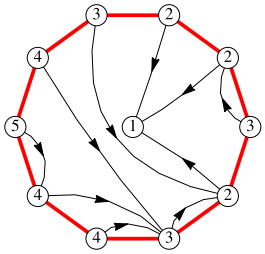

Figure 10. An example of the operation performed on a face of a labeled planar map in the definition of Ξ.

Theorem 1. *Schaeffer's prescription defines a bijection* $\Psi : \mathcal{Q}^{(l)} \to \mathcal{M}^{(l)}$ *with the following properties.*

(i) The number of edges of $\Psi(Q)$ *equals the number of faces* N *of* Q.
(ii) The number of faces of $\Psi(Q)$ *equals the number of local minima* $N_{\min}$ *of* Q.
(iii) The number of local maxima of $\Psi(Q)$ *equals the number of local maxima* $N_{\max}$ *of* Q.
(iv) The maximal label of $\Psi(Q)$ *equals the maximal label of* Q.
(v) The minimal label of $\Psi(Q)$ *equals the minimal label of* Q *plus one.*
(vi) The label on the root of $\Psi(Q)$ *equals the maximal label on the root edge of* Q.

Proof. Let us start by verifying properties (i)–(vi) for a quadrangulation Q. Properties (i) and (ii) have already been proven in lemma 1. To show (iii), let v be a vertex of Q with label t. Suppose that v is a local maximum on the quadrangulation, meaning that all its neighbors have smaller label, then it has maximal label in each of the adjacent faces. By inspection of the rules in figure 1(*a*) there is an edge of $\Psi(Q)$ leading away from v ending at a vertex with smaller or equal label for each adjacent face in Q. Therefore v is also a local maximum in $\Psi(Q)$. If v is not a local maximum, it is either a local minimum, in which case it does not appear as a vertex on $\Psi(Q)$, or both $t+1$ and $t-1$ appear as labels on its neighbors in Q. In the latter case there must be a simple face adjacent to v for which the coloring leads to an edge connecting v to a vertex with label $t+1$. Then v is not a local maximum of $\Psi(Q)$. Hence, the local maxima of Q and $\Psi(Q)$ coincide, which completes the proof of (iii). Moreover, (iv) follows from the fact that the vertices with maximal label are necessarily local maxima. Properties (v) is a consequence of the existence of at least one edge leading away from a vertex with minimal label, the end point of which is not a local minimum and therefore a vertex of $\Psi(Q)$. Finally, (vi) is a direct consequence of the construction.

To show that Ψ is a bijection, let us introduce a map $\Xi : \mathcal{M}^{(l)} \to \mathcal{Q}^{(l)}$, which we will later show to be the inverse of Ψ. Let $M \in \mathcal{M}^{(l)}$ be a labeled rooted planar map. For each face $\mathcal{F}$ of M the following operation is performed. Let $t_{\mathcal{F}}$ be the minimal label of the corners of $\mathcal{F}$. A new vertex is inserted in the interior of $\mathcal{F}$ with label $t_{\mathcal{F}} - 1$. Then for each corner a new edge is drawn. If the corner is labeled $t_{\mathcal{F}}$ it is connected to the new vertex, otherwise it is connected to the first corner with smaller label that one encounters when traversing the boundary of $\mathcal{F}$ in anti-clockwise order. See figure 10 for an example. Up to continuous deformations a unique way of drawing the new edges without crossing exists. To show this, it suffices to consider the edges leaving the corners with label larger than $t_{\mathcal{F}}$. Let e be such an edge with labels t and $t-1$ on its end points, then by construction the corners on the right-hand side of e have label larger or equal to t. Therefore they will never appear as end point of an edge starting at a

corner on the left-hand side of e. Hence, e can be drawn uniquely without crossing any other edges by keeping on its left-hand side both the new vertex and the previously drawn edges that start at corners on its left-hand side.

We claim that application of this operation to each face followed by deletion of the original edges gives a quadrangulation of the sphere. In order to show this let us consider the combined planar map M' containing both the old and new edges. Each face $\mathcal{F}'$ of M' is by construction bounded by exactly one old edge e. Let us orient e such that $\mathcal{F}'$ is on its right-hand side and denote the labels of the starting and end point of e by t_0 and t_1. As a result of the drawing rules, if $t_1 - t_0 = 1$ the degree of $\mathcal{F}'$ is 2, since there is a new edge with the same end points as e. If $t_1 - t_0 = 0$ the degree is 3, because both end points of e are connected by new edges to the same vertex with label $t_0 - 1$. Finally, it can be seen that when $t_1 - t_0 = -1$ the degree of $\mathcal{F}'$ is 4. Indeed, the end point of e is connected to the first corner c_1 with label $t_1 - 1$ encountered when running anti-clockwise around the face. But this is also the first corner with label $t_1 - 1$ after the first corner c_0 with label $t_1 = t_0 - 1$, to which the starting point of e is connected. By inspecting the degrees of the faces on either side of the edge e, we conclude that deletion of e in any case results in a face of degree 4. Hence, removing all old edges from M' gives a quadrangulation $\Xi(M)$, which is labeled by construction and can be rooted on the edge that was drawn from the root corner of M.

With the explicit construction of Ξ in hand it is straightforward to show that $\Psi \circ \Xi$ is the identity on $\mathcal{M}^{(l)}$. Indeed, as we have seen above, each face $\mathcal{F}$ of $\Xi(M)$ is formed by merging the faces on either side of an edge e of M with labels t_0 and t_1. If $t_0 = t_1$ the face $\mathcal{F}$ is confluent and e is the diagonal connecting the corners of $\mathcal{F}$ with largest label. Otherwise $\mathcal{F}$ is simple and e connects the corner with largest label to the next corner in clockwise direction around the face. In both cases these are precisely the colored edges that are to be drawn according to Schaeffer's prescription. Hence, $\Psi(\Xi(M))$ has the same edges as M, while the labels on M are unaffected by the operation and $\Psi(\Xi(M))$ is easily seen to be rooted at the root corner of M.

Finally let us prove that $\Xi \circ \Psi$ is the identity on $\mathcal{Q}^{(l)}$. To do this we show that all of the edges of a quadrangulation $Q \in \mathcal{Q}^{(l)}$ arise from the operation described above on the faces of the planar map $M = \Psi(Q)$. First of all, let e be an edge of Q that ends on a local minimum of Q. Since the starting point of e is not a local minimum, it corresponds to a corner of the face $\mathcal{F}$ of M that contains the end point of e in its interior. Since this corner has label exactly one larger than the vertex in the interior of $\mathcal{F}$, the edge e is indeed created by the operation. Now let e be an edge for which neither end point is a local minimum. We orient the edge such that its labels are of the form $(t, t-1)$. Since both end points of e are on M, e defines a chord of a face $\mathcal{F}$ of M. We claim that the corners of $\mathcal{F}$ that lie on the right-hand side of e have label larger or equal to t, which implies that the edge e is created by the operation of Ξ. To see this we inspect the quadrangle directly on the right-hand side of e. As shown in figure 11, three situations are possible, but in each case the corners of the quadrangle that correspond to new corners of $\mathcal{F}$ have label larger or equal to t. Moreover, the other edges of the quadrangle that lie in the same face $\mathcal{F}$ are again chords with labels larger or equal to those of e. The argument can be repeated with the new chords showing that no corners with label smaller than t can appear on the right-hand side of e. Hence, all edges of Q are created in the operation of Ξ on the faces of M and since the number of corners of M is equal to the number of edges of Q, Q can have no additional edges. □

The bijection Ψ of theorem 1 is quite useful as it gives rise to a whole bunch of specialized bijections when restricted to subsets of $\mathcal{Q}^{(l)}$ defined by certain restrictions on the properties (i)–(vi). For instance, the trivial bijection is obtained from theorem 1 by restricting the labels

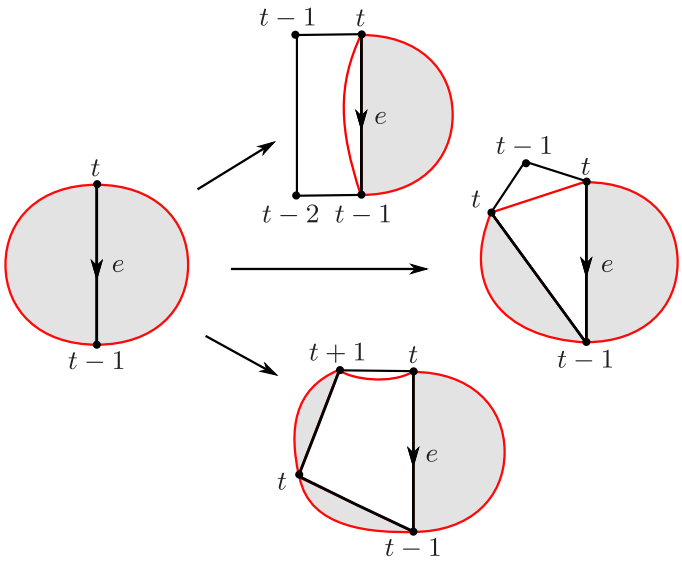

Figure 11. Illustration of the fact that the corners to the right of e have label larger than $t-1$. The red curve represents the boundary of the face $\mathcal{F}$, while the shaded areas represents the unknown tiling of the $\mathcal{F}$ by faces of Q.

on the quadrangulations to take the values 0 or 1. To retrieve the Cori–Vauquelin–Schaeffer bijection from section 2.2 we need the following simple lemma.

Lemma 2. *Let $M \in \mathcal{M}^{(l)}$ be a labeled rooted planar map. If M has a single local minimum labeled 0, then the labeling corresponds to the distance labeling to the vertex labeled 0. The same holds for labeled rooted quadrangulations, since $\mathcal{Q}^{(l)} \subset \mathcal{M}^{(l)}$.*

Proof. Each vertex of M with label $t > 0$ is not a local minimum and therefore has a 'descending' edge connecting it to a vertex of label $t-1$. Starting at a vertex with label $t > 0$ one can find a path of length t to the vertex with label 0 by repeatedly traversing descending edges. Since the labels differ by at most one along the edges, no shorter path exists. □

It follows from lemma 2 that the subset of $\mathcal{Q}^{(l)}$ given by quadrangulations Q with a single local minimum labeled 0 is in bijection with the set of rooted pointed quadrangulations. According to theorem 1 it is also in bijection with the set of labeled rooted planar maps with one face and minimal label 1, i.e. the set of rooted well-labeled trees. Moreover, property (iii) justifies the counting of the local maxima of $\Psi(Q)$ instead of the local maxima of Q used in section 3.

Instead of requiring a single local minimum one can also require a single local maximum labeled 0. In that case the labels on the quadrangulations Q represent minus the distance to the local maximum, again giving a subset of $\mathcal{Q}^{(l)}$ in bijection with the set of rooted pointed quadrangulations. But now according to theorem 1 this subset is in bijection with the set of labeled rooted planar maps M with a single local maximum with label 0. It follows, again from lemma 2, that the labels on M also correspond to minus the distance to the local maximum and are fixed by the choice of a distinguished vertex with label 0. We therefore have the following result, where we flipped the sign of all the labels.

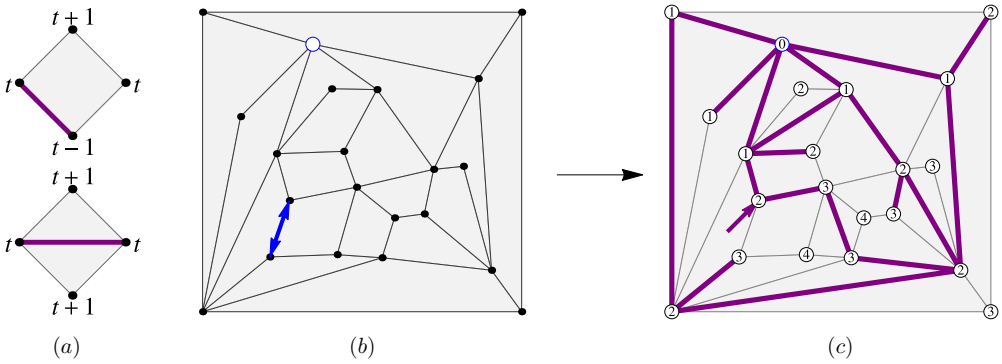

Figure 12. The prescription (*a*) opposite to Schaeffer's prescription gives a bijection between rooted pointed quadrangulations (*b*) and rooted pointed planar maps (*c*).

Theorem 2. *Application of the prescription in figure 12(a) to the distance labeling of a rooted pointed quadrangulation Q gives a planar map $\Phi(Q)$ with a distinguished vertex, which can be rooted at the corner containing the end point with smallest label of the root edge of Q. The map $\Phi : \mathcal{Q} \to \mathcal{M}$ is a bijection between the set $\mathcal{Q}$ of rooted pointed quadrangulations of the sphere and the set $\mathcal{M}$ of rooted pointed planar maps. It satisfies the following properties.*

(i) The number of edges of $\Phi(Q)$ equals the number of faces of Q.
(ii) The number of faces of $\Phi(Q)$ equals the number of local maxima $N_{\max}$ of Q.
(iii) The distance of the origin to the root vertex in $\Phi(Q)$ equals the distance of the origin to the closest end point of the root edge in Q.

Proof. See discussion above. Properties (i), (ii) and (iii) follow directly from properties (i), (ii) and (vi), respectively, of theorem 1. □

In figure 12(*c*) we have shown the result of the new coloring rules for the same quadrangulation as in figure 1.

As a consequence of theorem 2 the counting of rooted pointed quadrangulations with a fixed number of faces N and a fixed number of local maxima $N_{\max}$ coincides with the counting of rooted pointed planar maps with N edges and $N_{\max}$ faces[6]. In fact, we may conclude that the generalized CDT amplitudes appear as the natural scaling limit of random planar maps in which the number of faces is kept finite.

In section 4 we have studied the distribution of distances between the root and the origin in random rooted pointed quadrangulation with a certain number of local maxima. As a byproduct of this analysis we obtain expressions for the distribution of distances in random planar maps as a function of the number of edges and the number of faces.

Recall from section 4 that $z_0(t) - z_0(t-1)$, with $z_0(t)$ as in (26), is the generating function for the number of rooted pointed quadrangulations with N faces and n local maxima for which the origin is a distance t from the furthest end of the root edge. Hence, we find the generating function

$$z_t(g, \mathfrak{g}) := z_0(t+1) - z_0(t) = \sum_{N=0}^{\infty} \sum_{n=0}^{N+1} \mathcal{N}_t(N, n) g^N \mathfrak{g}^n \tag{52}$$

[6] Let us remark that combining Φ with the trivial bijection gives a bijection $\Phi_0^{-1} \circ \Phi$ of the set of rooted pointed quadrangulations onto itself. A quadrangulation with $N_{\max}$ local maxima is mapped to a quadrangulation with precisely $N_{\max}$ vertices at odd distance of the origin, which therefore also obey the same counting.

Table 1. The first few non-zero values of the number $\mathcal{N}_t(N, n)$ of rooted pointed maps with N edges, n faces and the origin at distance t from the root.

		$t=0$	$t=1$	$t=2$	$t=3$	$t=4$	$t=5$
$N=1$	$n=1$	1	1				
	$n=2$	1					
$N=2$	$n=1$	2	3	1			
	$n=2$	5	5				
	$n=3$	2					
$N=3$	$n=1$	5	9	5	1		
	$n=2$	22	34	10			
	$n=3$	22	22				
	$n=4$	5					
$N=4$	$n=1$	14	28	20	7	1	
	$n=2$	93	175	89	15		
	$n=3$	164	258	70			
	$n=4$	93	93				
	$n=5$	14					
$N=5$	$n=1$	42	90	75	35	9	1
	$n=2$	386	813	546	165	20	
	$n=3$	1030	1993	954	143		
	$n=4$	1030	1640	420			
	$n=5$	386	386				
	$n=6$	42					

for the number $\mathcal{N}_t(N, n)$ of rooted pointed quadrangulations with the origin exactly at distance t from the *closest* end of the root edge. According to theorem 2, property (iii), these quadrangulations are mapped by Φ exactly onto rooted pointed planar maps with N edges, n faces and the origin at distance t from the root, which are therefore also counted by $z_t(g, \mathfrak{g})$. It is a direct generalization of the generating function $z_{t=0}(g, \mathfrak{g})$ for rooted planar maps with N edges and n faces first derived by Tutte in [38]. On the other hand it generalizes the two-point functions for planar maps derived in [17, 21, 24] of which the simplest versions roughly correspond to $z_t(g, \mathfrak{g} = 1)$. By plugging the solutions to (18) and (27) into (26) one can explicitly compute the coefficients $\mathcal{N}_t(N, n)$. The first few non-zero values of $\mathcal{N}_t(N, n)$ are shown in table 1 and are checked to agree with a brute-force enumeration of all planar maps up to $N = 5$.

6. Loop identities

A process was studied in [10, 11] in which two universes merge and the resulting universe disappears into the vacuum. From a two-dimensional perspective, we consider the amplitude for surfaces with two boundary loops of length L_1 and L_2 respectively separated by a geodesic distance D (figure 13). In contrast to the case of the propagator, where all points on the final boundary are required to have a fixed distance to the initial boundary, here we only fix the minimal distance between the boundaries. To get a generalized CDT amplitude, one has to specify the time on the boundaries, which is taken to be constant T_1 and T_2 respectively. In order to get a continuous time function throughout the surface, the boundary times T_1 and T_2 and the distance D have to satisfy the inequality $|T_1 - T_2| \leqslant D$. The resulting amplitude is denoted by $G_{\lambda,\mathfrak{g}_s}(L_1, L_2; T_1, T_2; D)$.

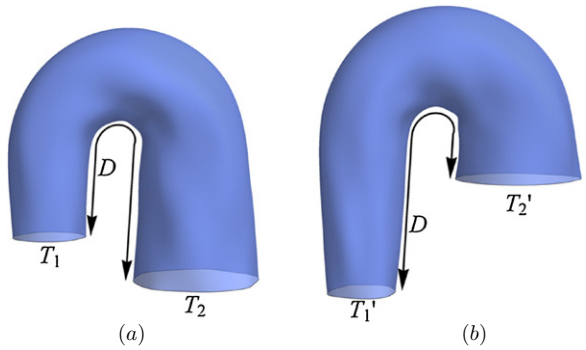

Figure 13. The two-loop amplitudes $G_{\lambda,\mathfrak{g}_s}(L_1, L_2; T_1, T_2; D)$.

In [10, 11] it was shown that $G_{\lambda,\mathfrak{g}_s}(L_1, L_2; T_1, T_2; D)$ can be expressed in terms of two propagators and a cap function. A non-trivial calculation showed that, quite remarkably, the amplitude $G_{\lambda,\mathfrak{g}_s}(L_1, L_2; T_1, T_2; D)$ does not depend on T_1 and T_2 at all,

$$G_{\lambda,\mathfrak{g}_s}(L_1, L_2; T_1, T_2; D) = G_{\lambda,\mathfrak{g}_s}(L_1, L_2; D) \quad (\text{provided } |T_1 - T_2| \leqslant D). \quad (53)$$

Even though the same ensemble of surfaces contributes to the loop–loop amplitudes with different initial times, like the ones in figure 13, this is non-trivial because the weight assigned to each surface depends on the number of local maxima of the time functions and therefore on the boundary times.

A similar identity can be derived for Euclidean two-dimensional gravity [13], in which case it can be understood as a consistency relation for the continuum amplitudes. From the discrete point of view, e.g. in terms of the quadrangulations discussed previously, it is clear that such an identity must hold since for $\mathfrak{g} = 1$ the contribution of each quadrangulations is independent of the labeling. In the following we will show that even for $\mathfrak{g} \neq 1$ the discrete two-loop amplitude $\mathcal{G}_{\mathfrak{g}}(l_1, l_2; t_1, t_2; d)$, which is the discrete analogue of $G_{\lambda,\mathfrak{g}_s}(L_1, L_2; T_1, T_2; D)$, is independent of t_1 and t_2. In fact, we will show that for any two pairs (t_1, t_2) and (t_1', t_2') there exists a bijection from the set of quadrangulations with two boundaries onto itself, such that a quadrangulation with a number of local maxima with respect to the pair (t_1, t_2) is mapped to a quadrangulation with the same number of local maxima with respect to the pair (t_1', t_2'). The continuum identity (53) and its discrete analogue are a direct consequence of the existence of such a bijection.

Before we consider quadrangulations with two boundaries, let us consider the set $\mathcal{Q}_d$ of rooted quadrangulations Q of the sphere with two marked vertices v_1 and v_2 separated by a distance d along the edges of Q. Given a pair of integers (t_1, t_2) satisfying $|t_1 - t_2| < d$ and $t_1 + t_2 + d$ even, one can label the vertices of the quadrangulation in a unique way such that the only local minima occur at the vertices v_i, which are labeled t_i, and the labels vary by exactly one along the edges. The labeling gives the distance to v_1 shifted by t_1 or the distance to v_2 shifted by t_2, depending on which one is smaller (see [36] for a similar construction). According to (the sign-flipped version of) theorem 1 the rooted labeled quadrangulation is mapped by Ψ to a rooted labeled planar map for which the only two local minimal are again v_i with label t_i. As for the quadrangulation the labeling on the planar map is the distance to v_1 shifted by t_1 or the distance to v_2 shifted by t_2, depending on which one is smaller. Hence, one obtains a rooted planar map $\Phi^d_{t_1,t_2}(Q)$ with two marked vertices, of which the labeling is canonical.

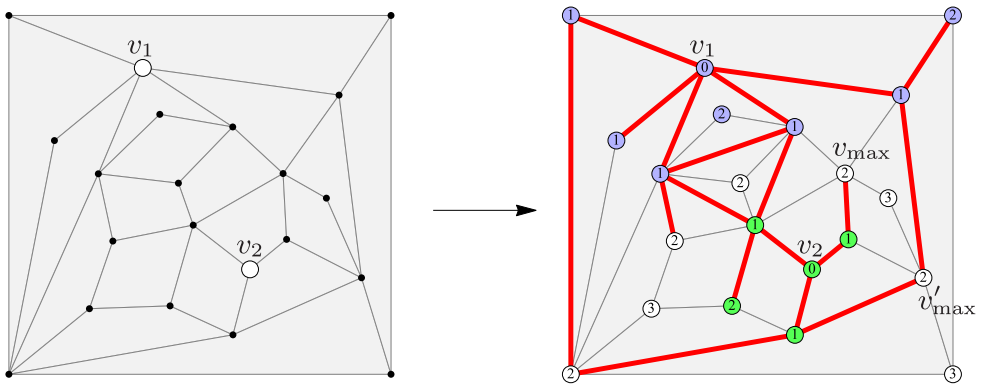

Figure 14. (*a*) An example of a quadrangulation Q with two marked vertices separated by a distance $d = 4$. (*b*) The planar map resulting from the canonical labeling with $t_1 = t_2 = 0$. The vertices of type 0, 1 and 2 are colored white, blue and green, respectively. Both the vertices $v_{\max}$ and $v'_{\max}$ are of type 0 and have label equal to $t_{\max} = 2$ (notice that there are three more vertices satisfying the same property). The vertex $v_{\max}$ is adjacent to a face containing both a type-1 vertex and a type-2 vertex which are connected in the planar map by the diagonal, hence giving rise to a path of length $d - 1$ connecting v_1 and v_2. The vertex $v'_{\max}$ on the other hand has a type-1 and type-2 vertex both followed by a type-0 vertex in its anti-clockwise sequence of neighbors. Therefore there is a path of length d passing via $v'_{\max}$.

Theorem 3. *For any pair of integers* (t_1, t_2) *satisfying* $d - |t_1 - t_2| \in \{2, 4, 6, \ldots\}$ *the map* $\Phi^d_{t_1,t_2} : \mathcal{Q}_d \to \mathcal{M}_d \cup \mathcal{M}_{d-1}$, *where* $\mathcal{M}_d$ *is the set of rooted planar maps with two marked vertices separated by a distance d, is a bijection.*

Proof. It follows from (the sign-flipped version of) theorem 1 that the set $\mathcal{Q}_{t_1,t_2}$ of rooted labeled quadrangulations with two local minima labeled t_1 and t_2 is in bijection with the set $\mathcal{M}_{t_1,t_2}$ of rooted labeled planar maps again with two local minima labeled t_1 and t_2. Any $Q \in \mathcal{Q}_{t_1,t_2}$ has a distance d between the local minima satisfying $d = |t_1 - t_2| + 2k$ for some $k \geqslant 1$, because of the bipartiteness of Q. This means that we have a natural bijection

$$\mathcal{Q}_{t_1,t_2} \longleftrightarrow \bigcup_{k=1}^{\infty} \mathcal{Q}_{d=|t_1-t_2|+2k}, \tag{54}$$

given by the canonical labeling discussed above. Likewise, any $M \in \mathcal{M}_{t_1,t_2}$ has a distance $d = |t_1 - t_2| + m$ for some $m \geqslant 1$ between its local minima. Therefore we have a natural bijection

$$\mathcal{M}_{t_1,t_2} \longleftrightarrow \bigcup_{m=1}^{\infty} \mathcal{M}_{d=|t_1-t_2|+m} = \bigcup_{k=1}^{\infty} (\mathcal{M}_{d=|t_1-t_2|+2k-1} \cup \mathcal{M}_{d=|t_1-t_2|+2k}). \tag{55}$$

To show that $\Phi^d_{t_1,t_2}$ defines a bijection between the individual sets $\mathcal{Q}_{d=|t_1-t_2|+2k}$ and $\mathcal{M}_{d=|t_1-t_2|+2k-1} \cup \mathcal{M}_{d=|t_1-t_2|+2k}$ appearing on the right-hand side of (54) and (55) it is sufficient to check that $\Phi^d_{t_1,t_2}(\mathcal{Q}_d) \subset \mathcal{M}_d \cup \mathcal{M}_{d-1}$.

Given a rooted quadrangulation $Q \in \mathcal{Q}_d$ with two marked vertices separated by a distance d (see figure 14(*a*) for an example with $d = 4$). We will show that v_1 and v_2 are separated by d or $d - 1$ edges in the planar map $M = \Phi^d_{t_1,t_2}(Q)$. For convenience we assign a *type* to vertices v in the quadrangulation Q according to their distances $d(v, v_i)$ to v_1 and v_2. A vertex v is of

type 1 if $d(v, v_1) + t_1 < d(v, v_2) + t_2$, of type 2 if $d(v, v_1) + t_1 > d(v, v_2) + t_2$, and of type 0 in case of equality (see figure 14(*b*)). For $i = 1, 2$ a type-i vertex v labeled t that is not a local maximum has a distance $t - t_i$ in the planar map to v_i. Due to triangle inequalities all vertices labeled $t < t_{\max} := (t_1 + t_2 + d)/2$ are either of type 1 or type 2. Any path connecting v_1 and v_2 in the planar map must include a vertex labeled $t_{\max} - 1$ of type 1 and one of type 2, and therefore its length is at least $d-1$. Since the distance between v_1 and v_2 in the quadrangulation is d, there must exist at least one vertex $v_{\max}$ with $d(v_{\max}, v_1) + t_1 = d(v_{\max}, v_2) + t_2 = t_{\max}$, which is the vertex of maximal label on a geodesic connecting v_1 and v_2 (see figure 14(*b*)). Let us consider the cycle of neighbors of $v_{\max}$ in Q in anti-clockwise order. They come in three types: vertices of type 0 labeled $t_{\max} + 1$, vertices of type 1, respectively of type 2, labeled $t_{\max} - 1$. Moreover, at least one vertex of both type 1 and type 2 must occur. Now there are two possibilities for the cycle: either a type-1 vertex is adjacent to a type-2 vertex, or both a type-1 vertex and a type-2 vertex are followed by a type-0 vertex (examples of both situations are indicated by $v_{\max}$ and $v'_{\max}$ in figure 14(*b*)). In the first case the type-1 vertex and the type-2 vertex are opposite corners of a confluent face and are therefore connected by an edge in the planar map. Hence, there is a path of length $d - 1$ connecting v_1 and v_2. In the second case $v_{\max}$ is connected by an edge in the planar map to both a type-1 vertex and a type-2 vertex, resulting in a path of length d. Hence, $\Phi^d_{t_1,t_2}(\mathcal{Q}_d) \subset \mathcal{M}_d \cup \mathcal{M}_{d-1}$. □

From the bijection $\Phi^d_{t_1,t_2}$ we can easily construct the bijection

$$\Phi^d_{t'_1,t'_2}{}^{-1} \circ \Phi^d_{t_1,t_2} : \mathcal{Q}_d(N) \to \mathcal{Q}_d(N), \quad |t_1 - t_2|, |t'_1 - t'_2| \in \{d-2, d-4, \ldots\}, \tag{56}$$

which maps the set of rooted quadrangulations with two marked points separated by a distance d to itself. A quadrangulation with a number $N_{\max}$ of local maxima of the canonical labeling w.r.t. (t_1, t_2) is mapped to a quadrangulation with $N_{\max}$ local maxima of the canonical labeling w.r.t. (t'_1, t'_2).

The bijection (56) can be extended to quadrangulations with two boundaries instead of two marked points by gluing disks to the boundaries as we did for the propagator in section 4. We consider quadrangulations Q with two boundaries, one of length $2l_1$ labeled alternatingly by t_1 and $t_1 + 1$, and another of length $2l_2$ labeled t_2 and $t_2 + 1$. We fix the smallest distance between the points labeled t_1 on the first boundary and the points labeled t_2 on the second boundary to be d, subject to the same inequalities as above, i.e. $d - |t_1 - t_2|$ positive and even. By gluing disks constructed from l_i simple faces to the boundaries, a quadrangulation is obtained with two marked vertices v_i labeled $t_i - 1$ and separated by a distance $d + 2$. The bijection (56) leaves invariant the structure of the quadrangulation in the direct neighborhood of v_i, and therefore the disks can be removed again after the bijection to obtain a quadrangulation with different labels (t'_1, t'_2) on its boundaries.

It follows immediately that the discrete two-loop amplitude $\mathcal{G}_{\mathfrak{g}}(l_1, l_2; t_1, t_2; d)$, i.e. the generating function for such quadrangulations including a factor of $\mathfrak{g}$ for each local maximum of the canonical labeling, is independent of t_1 and t_2 (as long as $d - |t_1 - t_2|$ is positive and even).

7. Triangulations

For the sake of completeness we will show that most constructions in this paper can also be carried out for triangulations. As we will see, the analogues of the bijections described in section 2 are not as simple for triangulations but still manageable. The bijection we will use is a special case of the Bouttier–Di Francesco–Guitter bijection between arbitrary planar maps and *labeled mobiles* introduced in [18]. In a slightly different formulation it was used by

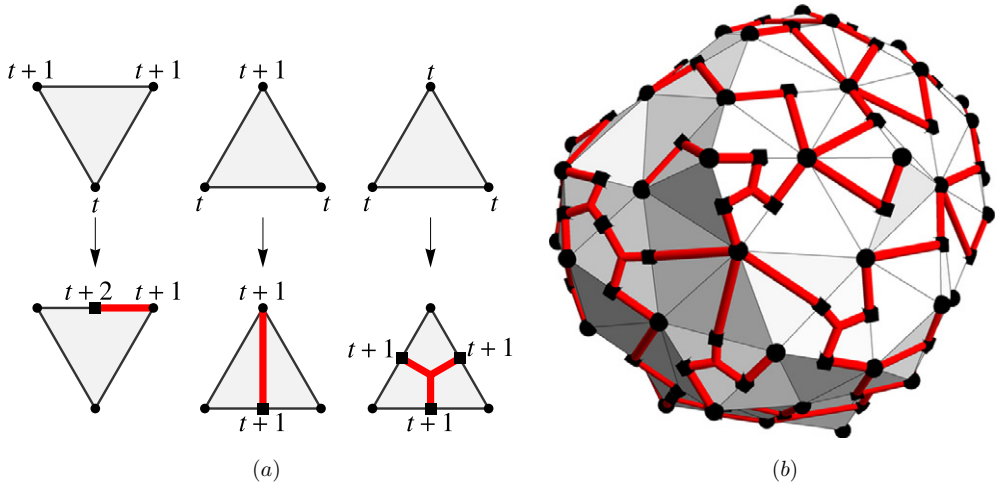

Figure 15. (*a*) The rules for a 'down' triangle, an 'up' triangle, and a 'flat' triangle respectively. (*b*) An example of the application of the rules to a triangulation of the sphere.

Le Gall in [32] to prove that random triangulations and random quadrangulations as metric spaces converge in a quite general way to the same continuum object, known as the *Brownian map*.

The bijection for triangulations can be understood as a special case of the Cori–Vauquelin–Schaeffer bijection for quadrangulations. Given a triangulation of the sphere with N triangles and one vertex marked as the origin, one can label all the vertices according to their distance to the origin along the edges. A new vertex labeled $t+1$ is inserted in the middle of each edge connecting vertices of equal label t. Each triangle with equal labels t, called a *flat* triangle, is subdivided into three faces by connecting each of the three new vertices on its edges to a new vertex labeled $t+2$ in the center of the triangle. The resulting planar map is a quadrangulation labeled by the distance to the origin. It is convenient to keep track of the vertices belong to the triangulation (type 1), the vertices lying on the edges of the triangulation (type 2), and the vertices in the centers of the flat triangles (type 3). The first two types are depicted in figure 15 by disks and squares respectively, while the type-3 vertices correspond to the unmarked intersections.

The application of Schaeffer's prescription (figure 1(*a*)) to the resulting quadrangulation turns out to be equivalent to the prescription in figure 15(*a*) for the triangles. Not all quadrangulations arise from triangulations, hence a limited class of labeled trees will appear. Before discussing this class, it is convenient to switch to the rooted versions of the triangulations and trees, like in section 2.2. A triangulation is rooted by distinguishing an edge, which for simplicity we demand to connect vertices of different label[7]. Since this edge appears in the quadrangulation with a vertex of type 1 at its end point with largest label, the tree is naturally rooted at this vertex. From the way the triangles in figure 15(*a*) can be glued, it can be seen that the class of rooted, labeled trees satisfies the following rules (see [32]). The root is of type 1. A vertex of type 1 labeled t has zero or more children of type 2 labeled t or $t+1$. A vertex of type 2 labeled t has either one child of type 1 labeled t or $t-1$, or two children of type 2 labeled t. Notice that in the latter case we regard the two type-2 vertices of a flat

[7] See [32] for the general case where any oriented edge can be used as root.

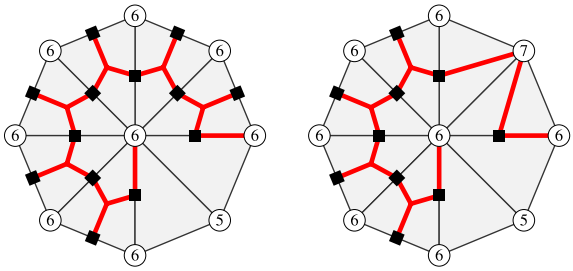

Figure 16. An example of a vertex that is (*a*) a local maximum and (*b*) one that is not.

triangle to be directly connected to the other type-2 vertex, instead of keeping track of the type-3 vertex in between.

One would like to identify vertices that are local maxima of the labeling, which in this case means that they have label greater than or equal to their neighbors in the triangulation. In the case of quadrangulations such property of a vertex could be established locally from the labeled tree just by considering the labels of tree edges incident to it. Unfortunately this is not the case for triangulation, as can be seen from the examples in figure 16. Whether or not a vertex is a local maximum may depend on the structure in the tree an arbitrary distance away from that vertex. Assigning couplings to local maxima is an inherently non-local procedure from the point of view of the labeled trees, and therefore quite impractical to treat analytically.

Instead, we will show that one can get a similar model by assigning couplings to saddle-point configurations in the triangulation. In fact, we will introduce two couplings, $\mathfrak{g}_1$ and $\mathfrak{g}_2$, related to two different ways in which saddle points can occur. We assign a coupling $\mathfrak{g}_1$ to each type-1 vertex labeled t that is connected to more than one type-2 vertex labeled $t+1$. In the triangulation this corresponds to a vertex labeled t for which the labels of its neighbors run from t to $t-1$ and back to t at least twice when walking around the vertex. We also assign a coupling $\mathfrak{g}_2$ to each type-2 vertex labeled t that is not connected to a type-1 vertex labeled $t-1$. This corresponds to an edge labeled (t,t) which is not shared by a *down* triangle (see figure 15(*a*)).

Both these configurations are independent and correspond to configurations that are absent in causal triangulations. If we set both couplings to zero and consider rooted, labeled trees for which all edges connecting to the root have constant label, we get exactly causal triangulations rooted at the 'top', as in section 2.3. Therefore it makes sense to search for generalized CDT in the continuum limit by scaling the couplings $\mathfrak{g}_1$ and $\mathfrak{g}_2$ to zero.

Let us introduce the generating functions $z_{i,\sigma}(g)$ for trees with a vertex of type $i=1,2$ at the root. The label $\sigma=-,0,+$ indicates whether the tree can be appear as a subtree of a larger tree with an edge of label σ pointing toward the root of the subtree. As can be deduced from the prescription in figure 15(*a*), only four of these occur, namely $z_{1,-}$, $z_{1,0}$, $z_{2,0}$, and $z_{2,+}$. They satisfy the recurrence relations

$$z_{1,-}=\frac{1-\mathfrak{g}_1}{1-gz_{2,0}}+\frac{\mathfrak{g}_1}{1-gz_{2,+}-gz_{2,0}}, \tag{57}$$

$$z_{1,0}=\frac{1-\mathfrak{g}_1}{1-gz_{2,0}}+gz_{2,+}\frac{1-\mathfrak{g}_1}{(1-gz_{2,0})^2}+\frac{\mathfrak{g}_1}{1-gz_{2,+}-gz_{2,0}}, \tag{58}$$

$$z_{2,0} = g\big(z_{1,-} + \mathfrak{g}_2\big(z_{1,0} + z_{2,0}^2\big)\big), \tag{59}$$

$$z_{2,+} = g\big(z_{1,-} + z_{1,0} + z_{2,0}^2\big). \tag{60}$$

If we scale $g = 1/2(1 - \lambda\epsilon^2/2)$ and $\mathfrak{g}_i = \mathfrak{g}_{s,i}\epsilon^3$ we find that the generating functions scale as $z_{1,-} = 2(1 - Z_{1,-}\epsilon)$, $z_{1,0} = Z_{1,0}/\epsilon$, $z_{2,0} = 1 - Z_{2,0}\epsilon$, and $z_{2,+} = Z_{2,+}/\epsilon$, satisfying

$$Z_{1,0} = 2Z_{2,+} = \frac{5}{2Z_{2,0}}, \quad Z_{1,-} = Z_{2,0} \tag{61}$$

$$Z_{2,0}^3 - \lambda Z_{2,0} + \frac{5}{4}\mathfrak{g}_{s,2} = 0. \tag{62}$$

Interestingly, only the coupling $\mathfrak{g}_2$ survives in the continuum limit and produces the generalized CDT coupling $\mathfrak{g}_s$ up to a factor of 5/4.[8]

The cup function $w(g, y)$ with a constant distance between the boundary and the origin is obtained simply by combining independent trees generated by $z_{2,0}$,

$$w(g, y) = \sum_{l=0}^{\infty} z_{2,0}(g)^l y^l = \frac{1}{1 - y\, z_{2,0}(g)}. \tag{63}$$

Taking the continuum limit of this expression, we arrive at the same result as for quadrangulations (24) with Z_1 replaced by $Z_{2,0}$, which obeys the same equation (62).

8. Discussion and conclusions

The model of two-dimensional quantum gravity denoted generalized causal dynamical triangulations was originally introduced as a continuum model of geometries. The equations which determined the disk function and the two-loop function were found from simple consistency relations which had to be satisfied for the ensemble of geometries in question. Only afterward an actual realization of this ensemble in terms of discrete triangulations was studied, from which a scaling limit could be found by taking the link length to zero. The purpose of this paper has been to present another discrete realization of the model, in terms of labeled quadrangulations, which could be studied in more detail and be solved already largely at the discrete level. Let us summarize some of the main results reported in this paper.

(1) There exists a bijection Φ from the set of rooted pointed quadrangulations of the sphere with N faces to the set of rooted pointed planar maps with N edges such that the distance labeling of a quadrangulation Q is mapped to the distance labeling of $\Phi(Q)$, and such that if Q has n local maxima with respect to the distance labeling then $\Phi(Q)$ has n faces.
(2) An explicit generating function has been obtained for the number of rooted pointed quadrangulations of the sphere which have N faces and n local maxima with respect to the distance labeling and where the root is a distance t from the origin. This is also the generating function for the number of rooted pointed planar maps with N edges and n faces and where the root is a distance t from the origin.
(3) We have shown that the generating functions for the ensemble of planar maps possess a well-defined scaling limit as $N \to \infty$, while keeping n fixed. In this limit one obtains precisely the amplitudes of the generalized CDT model of two-dimensional quantum gravity, which have been established in the physics literature. Moreover, we have found a new explicit formula for the two-point function of generalized CDT.

[8] This slightly awkward factor of 5/4 can be seen to be due to the presence of flat triangles for small but non-zero $\mathfrak{g}_{s,2}$. If one assigns yet another coupling $\mathfrak{g}_3$ to each flat triangle, which amounts to inserting $\mathfrak{g}_3$ in front of the $z_{2,0}^2$-terms in (59) and (60), and one scales $\mathfrak{g}_3$ to zero at least linearly in ϵ, the factor of 5/4 will disappear and we get exactly $\mathfrak{g}_{s,2} = \mathfrak{g}_s$.

Figure 17. A random pointed quadrangulation with the origin indicated by a black dot and three local maxima. The associated planar map drawn on top of the quadrangulation has three faces, as indicated by the coloring, of which the interiors may be viewed as baby universes.

(4) We have shown that a loop identity first discovered by Kawai *et al* in the continuum limit of DT, and seemingly related to the Virasoro algebra of the corresponding continuum quantum Liouville theory, is valid even at the combinatorial level of generalized CDT. This loop identity is a consequence of the existence of a range of bijections between quadrangulations with two marked points and planar maps with two marked points.

Let us make some remarks on the physical interpretation of generalized CDT as 2D gravity with spatial topology change. In the two-dimensional CDT model 'space' has the topology of S^1 and a two-dimensional CDT surface with the topology of a cylinder allows a 'time' foliation. In generalized CDT one allows the space with topology S^1 to split into several S^1s as a function of time. Each of these S^1s develops independently and its splitting off can be viewed as the creation of a baby universe. As a function of time (or distance) we allow a finite number of these baby universes to be created and eventually to vanish again ('decay into the vacuum' in physics jargon). Each spacetime point has a distance to the initial spatial S^1 and this distance has a local maximum where a baby universe vanishes. In this way we were led to study quadrangulations with a fixed number of local maxima of the distance with respect to the initial spatial S^1. The outcome of our analysis is that this is combinatorially equivalent to the study of planar maps with a fixed number of faces and the generalized CDT model was obtained as a specific scaling limit of these planar maps. In the planar map representation a baby universe is represented as a face and the spacetime volume of the baby universe is proportional to the degree of the face (see figure 17 for an example). In fact, inspection of the construction of the planar map shows that a face of degree d covers exactly $d/2$ quadrangles.

This model may be compared with [33] (see also [29]), where random planar maps are studied with non-trivial weights on the degrees of the faces. By choosing different asymptotic laws for these weights, it was shown that different continuum limits are obtained with Hausdorff dimensions anywhere between 2 and 4. It would be interesting to see whether putting non-trivial (hence non-local) weights on the volumes of baby universes leads to continuum limits that in a similar fashion continuously interpolate between DT and CDT, and if such weights can be given an interpretation in terms of continuum physics.

One should keep in mind, however, that the geometry studied in [33] is the intrinsic geometry of the planar maps, which differs from the geometry of the associated quadrangulations. Indeed, only geodesic distances to the origin are preserved under the

bijection. General methods to study distances between arbitrary points in generalized CDT, or even in ordinary CDT, are currently lacking. This means that we have not yet arrived at a complete understanding of the two-dimensional continuum geometry of generalized CDT.

Finally, let us mention that recently it has been shown that one can obtain new multi-critical scaling relations in the generalized CDT ensemble of graphs if one combines triangles with quadrangles with negative weights ([3] and [14, 15]). This is very similar to the now 'classical' situation for the DT ensemble where a similar combination of weights for triangles and quadrangles allowed one to obtain a scaling limit different from the standard DT limit as well as a different distance function ([27] and [17]). It should be possible to apply the techniques in [17] to the generalized CDT ensemble and obtain the corresponding distance functions.

Acknowledgments

The authors acknowledge support from the ERC-Advance grant 291092, 'Exploring the Quantum Universe' (EQU). JA acknowledges support of FNU, the Free Danish Research Council, from the grant 'quantum gravity and the role of black holes'.

References

[1] Agishtein M and Migdal A 1992 Simulations of four-dimensional simplicial quantum gravity as dynamical triangulation *Mod. Phys. Lett.* A **07** 1039–61
[2] Ambjørn J, Durhuus B and Jonsson T 1997 *Quantum Geometry : A Statistical Field Theory Approach (Cambridge Monographs on Mathematical Physics)* (Cambridge: Cambridge University Press)
[3] Ambjørn J, Glaser L, Görlich A and Sato Y 2012 New multicritical matrix models and multicritical 2d CDT *Phys. Lett.* B **712** 109–14 (arXiv:1202.4435)
[4] Ambjørn J, Görlich A, Jurkiewicz J and Loll R 2012 Nonperturbative quantum gravity *Phys. Rep.* **519** 127–210 (arXiv:1203.3591)
[5] Ambjørn J and Jurkiewicz J 1992 Four-dimensional simplicial quantum gravity *Phys. Lett.* B **278** 42–50
[6] Ambjørn J, Jurkiewicz J and Loll R 2001 Dynamically triangulating Lorentzian quantum gravity *Nucl. Phys.* B **610** 347–82 (arXiv:hep-th/0105267)
[7] Ambjørn J, Jurkiewicz J and Watabiki Y 1995 On the fractal structure of two-dimensional quantum gravity *Nucl. Phys.* B **454** 313–42 (arXiv:hep-lat/9507014)
[8] Ambjørn J and Loll R 1998 Non-perturbative Lorentzian quantum gravity, causality and topology change *Nucl. Phys.* B **536** 407–34 (arXiv:hep-th/9805108)
[9] Ambjørn J, Loll R, Watabiki Y, Westra W and Zohren S 2008 A matrix model for 2D quantum gravity defined by causal dynamical triangulations *Phys. Lett.* B **665** 252–6 (arXiv:0804.0252)
[10] Ambjørn J, Loll R, Watabiki Y, Westra W and Zohren S 2008 A string field theory based on causal dynamical triangulations *J. High Energy Phys.* JHEP05(2008)032 (arXiv:0802.0719)
[11] Ambjørn J, Loll R, Westra W and Zohren S 2007 Putting a cap on causality violations in causal dynamical triangulations *J. High Energy Phys.* JHEP12(2007)017 (arXiv:0709.2784)
[12] Ambjørn J and Watabiki Y 1995 Scaling in quantum gravity *Nucl. Phys.* B **445** 129–42 (arXiv:hep-th/9501049)
[13] Aoki H, Kawai H, Jun N and Tsuchiya A 1996 Operator product expansion in two-dimensional quantum gravity *Nucl. Phys.* B **474** 512–28 (arXiv:hep-th/9511117)
[14] Atkin M R and Zohren S 2012 An analytical analysis of CDT coupled to dimer-like matter *Phys. Lett.* B **712** 445–50 (arXiv:1202.4322)
[15] Atkin M R and Zohren S 2012 On the quantum geometry of multi-critical CDT *J. High Energy Phys.* JHEP11(2012)037 (arXiv:1203.5034)
[16] Bettinelli J 2011 Scaling limit of random planar quadrangulations with a boundary arXiv:1111.7227
[17] Bouttier J, Di Francesco P and Guitter E 2003 Geodesic distance in planar graphs *Nucl. Phys.* B **663** 535–67 (arXiv:cond-mat/0303272)
[18] Bouttier J, Francesco P Di and Guitter E 2004 Planar maps as labeled mobiles *Electron. J. Comb.* **11** R69 (arXiv:math/0405099)

[19] Bouttier J and Guitter E 2008 The three-point function of planar quadrangulations *J. Stat. Mech.: Theory Exp.* **2008** P07020 (arXiv:0805.2355)
[20] Bouttier J and Guitter E 2009 Distance statistics in quadrangulations with a boundary, or with a self-avoiding loop *J. Phys. A: Math. Theor.* **42** 465208 (arXiv:0906.4892)
[21] Bouttier J and Guitter E 2012 Planar maps and continued fractions *Commun. Math. Phys.* **309** 623–62 (arXiv:1007.0419)
[22] Chassaing P and Schaeffer G 2004 Random planar lattices and integrated superBrownian excursion *Probab. Theory Relat. Fields* **128** 161–212 (arXiv:math/0205226)
[23] Curien N and Miermont G 2012 Uniform infinite planar quadrangulations with a boundary arXiv:1202.5452
[24] Di Francesco P 2005 Geodesic distance in planar graphs: an integrable approach *Ramanujan J.* **10** 153–86 (arXiv:math/0506543)
[25] Di Francesco P, Guitter E and Kristjansen C 2000 Integrable 2D Lorentzian gravity and random walks *Nucl. Phys.* B **567** 515–53 (arXiv:hep-th/9907084)
[26] Durhuus B, Jonsson T and Wheater J F 2010 On the spectral dimension of causal triangulations *J. Stat. Phys.* **139** 859–81 (arXiv:0908.3643)
[27] Gubser S S and Klebanov I R 1994 Scaling functions for baby universes in two-dimensional quantum gravity *Nucl. Phys.* B **416** 827–49 (arXiv:hep-th/9310098)
[28] Ishibashi N and Kawai H 1994 String field theory of $c \leqslant 1$ noncritical strings *Phys. Lett.* B **322** 67–78 (arXiv:hep-th/9312047)
[29] Janson S and Stefansson S O 2012 Scaling limits of random planar maps with a unique large face arXiv:1212.5072
[30] Kawai H, Kawamoto N, Mogami T and Watabiki Y 1993 Transfer matrix formalism for two-dimensional quantum gravity and fractal structures of space-time *Phys. Lett.* B **306** 19–26 (arXiv:hep-th/9302133)
[31] Krikun M and Yambartsev A 2012 Phase transition for the Ising model on the critical Lorentzian triangulation *J. Stat. Phys.* **148** 422–39 (arXiv:0810.2182)
[32] Le Gall J-F 2011 Uniqueness and universality of the Brownian map arXiv:1105.4842
[33] Le Gall J-F and Miermont G 2011 Scaling limits of random planar maps with large faces *Ann. Probab.* **39** 1–69 (arXiv:0907.3262)
[34] Le Gall J-F and Miermont G 2011 Scaling limits of random trees and planar maps arXiv:1101.4856
[35] Malyshev V, Yambartsev A and Zamyatin A 2001 Two-dimensional Lorentzian models *Mosc. Math. J.* **1** 439–56
[36] Miermont G 2009 Tessellations of random maps of arbitrary genus *Ann. Sci. l'Ecole Norm. Supér.* **42** 725–81 (arXiv:0712.3688)
[37] Schaeffer G 1998 Conjugaison d'arbres et cartes combinatoires aleatoires *PhD Thesis* L'Université Bordeaux
[38] Tutte W T 1968 On the enumeration of planar maps *Bull. Am. Math. Soc.* **74** 64–74